

AD-A164 280

BASELINE DESIGN OF A 5-7 KJ KRF LASER FACILITY FOR
DIRECT ILLUMINATION ICF EXPERIMENTS(U) NAVAL RESEARCH
LAB WASHINGTON DC R H LEHMBERG ET AL 31 DEC 85

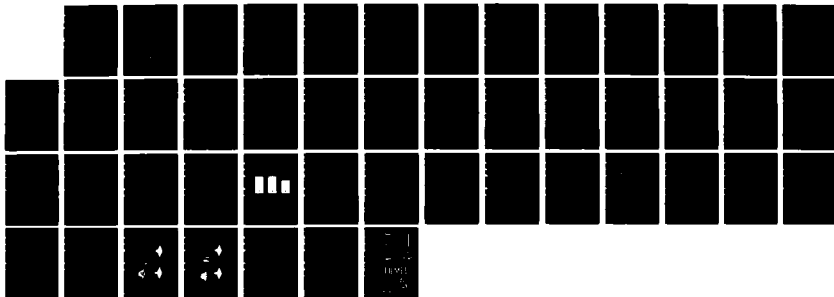
1/1

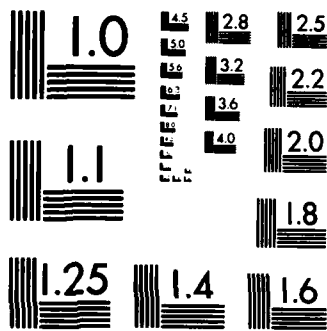
UNCLASSIFIED

NRL-MR-5713

F/G 18/1

ML





MICROCOPY RESOLUTION TEST CHART
NBS-1963-A

2

NRL Memorandum Report 5713

Baseline Design of a 5-7 kJ KrF Laser Facility for Direct Illumination ICF Experiments

R.H. LEHMBERG, S.P. OBENSCHAIN, AND A.J. SCHMITT

*Laser Plasma Branch
Plasma Physics Division*

December 31, 1985

AD-A164 280

DTIC FILE COPY



Handwritten initials and a stamp, possibly 'RHC' or similar, with a date 'DEC 31 1985'.

NAVAL RESEARCH LABORATORY
Washington, D.C.

Approved for public release; distribution unlimited.

96

SECURITY CLASSIFICATION OF THIS PAGE

AD-A164 210

REPORT DOCUMENTATION PAGE

1a. REPORT SECURITY CLASSIFICATION UNCLASSIFIED		1b. RESTRICTIVE MARKINGS	
2a. SECURITY CLASSIFICATION AUTHORITY		3. DISTRIBUTION / AVAILABILITY OF REPORT	
2b. DECLASSIFICATION / DOWNGRADING SCHEDULE		Approved for public release; distribution unlimited.	
4. PERFORMING ORGANIZATION REPORT NUMBER(S) NRL Memorandum Report 5713		5. MONITORING ORGANIZATION REPORT NUMBER(S)	
6a. NAME OF PERFORMING ORGANIZATION Naval Research Laboratory	6b. OFFICE SYMBOL (If applicable) Code 4730	7a. NAME OF MONITORING ORGANIZATION	
6c. ADDRESS (City, State, and ZIP Code) Washington, DC 20375-5000		7b. ADDRESS (City, State, and ZIP Code)	
8a. NAME OF FUNDING / SPONSORING ORGANIZATION U.S. Department of Energy	8b. OFFICE SYMBOL (If applicable) DP-23	9. PROCUREMENT INSTRUMENT IDENTIFICATION NUMBER	
8c. ADDRESS (City, State, and ZIP Code) Office of Inertial Fusion (DP-23) Washington, DC 20545		10. SOURCE OF FUNDING NUMBERS	
		PROGRAM ELEMENT NO. DOE	PROJECT NO. A108-79DP 40092
		TASK NO.	WORK UNIT ACCESSION NO.
			47-0859-00
11. TITLE (Include Security Classification) Baseline Design of a 5-7 kJ KrF Laser Facility for Direct Illumination ICF Experiments			
12. PERSONAL AUTHOR(S) Lehmburg, R.H., Obenschain, S.P., and Schmitt, A.J.			
13a. TYPE OF REPORT Interim	13b. TIME COVERED FROM TO	14. DATE OF REPORT (Year, Month, Day) 1985 December 31	15. PAGE COUNT 47
16. SUPPLEMENTARY NOTATION			
17. COSATI CODES		18. SUBJECT TERMS (Continue on reverse if necessary and identify by block number)	
FIELD	GROUP	SUB-GROUP	
19. ABSTRACT (Continue on reverse if necessary and identify by block number)			
<p>This report presents the baseline design for a 48 channel angularly-multiplexed KrF laser system, using amplifier modules similar to those in the AURORA laser at Los Alamos National Laboratory. With output energies of 5-7 kJ, pulsewidths \approx 5 ns, and broadband ($> 20 \text{ cm}^{-1}$) capabilities, the proposed system is intended primarily for laser-plasma experiments related to direct-drive inertial confinement fusion. The design incorporates the NRL induced spatial incoherence (ISI) technique into each beam in order to achieve the smoothly-varying and controllable irradiation profiles essential to the direct-drive approach. The option of using stimulated Raman scattering to improve the beam quality prior to the ISI echelons is also discussed.</p>			
20. DISTRIBUTION / AVAILABILITY OF ABSTRACT <input type="checkbox"/> UNCLASSIFIED/UNLIMITED <input checked="" type="checkbox"/> SAME AS RPT <input type="checkbox"/> DTIC USERS		21. ABSTRACT SECURITY CLASSIFICATION UNCLASSIFIED	
22a. NAME OF RESPONSIBLE INDIVIDUAL Robert Lehmburg		22b. TELEPHONE (Include Area Code) (202) 767-2730	22c. OFFICE SYMBOL Code 4730

DD FORM 1473, 84 MAR

83 APR edition may be used until exhausted.
All other editions are obsolete

SECURITY CLASSIFICATION OF THIS PAGE

CONTENTS

I.	INTRODUCTION	1
II.	ANGULARLY MULTIPLEXED KrF LASERS	3
III.	BASELINE DESIGN	4
	A. Encoding Optics	5
	B. Amplifier Chain	6
	C. Decoding Optics	8
	D. ISI and Target Focusing Optics	9
	E. Optical Alignment and Stability Requirements	10
IV.	RAMAN BEAM COMBINATION	11
V.	SUMMARY, MANAGEMENT, AND SCHEDULE	12
	APPENDIX A — Fresnel Diffraction From a Square Aperture	13
	APPENDIX B — Primary Aberrations of Spherical Mirrors and Lenses	17
	REFERENCES	20

Accession For	
NTIS GRA&I	<input checked="" type="checkbox"/>
DTIC TAB	<input type="checkbox"/>
Unannounced	<input type="checkbox"/>
Justification	<input type="checkbox"/>
By _____	
Dist _____	
Avail _____	
Dist _____	
A-1	



BASELINE DESIGN OF A 5-7 KJ KRF LASER FACILITY FOR DIRECT ILLUMINATION ICF EXPERIMENTS

I. INTRODUCTION

In the effort to achieve direct drive laser fusion, it has become apparent in recent years that short optical wavelengths (e.g., $< 1/2 \mu\text{m}$) offer several advantages over the $1 \mu\text{m}$ illumination used in earlier experiments. Shorter wavelengths allow improved target absorption,^{1,2} lower preheat from hot electrons,^{2,3} and higher rocket implosion efficiencies.³ The latter advantage is underscored by recent simulations performed at NRL, which predict $1/4 \mu\text{m}$ rocket implosion efficiencies as high as 15% on shell targets of 10:1 aspect ratio.⁴ Other theoretical work at NRL suggests an important additional advantage of short wavelength; namely, a significant reduction in the exponential growth rate of the Rayleigh-Taylor (R-T) instability.^{4,5} This theory predicts that while the R-T growth rate with $1 \mu\text{m}$ light is typically $1/2$ the classical value, it reduces to $\sim 0.3 \times$ the classical value with $1/4 \mu\text{m}$ light.

Short wavelength light has the disadvantage that it places a greater constraint upon laser beam uniformity. To achieve high energy gain, inertial confinement fusion requires ablation pressures uniform to within a few percent.⁶ To accomplish this with nonuniform laser beams, the direct-drive concept has in the past relied primarily upon the "cloudy day" effect, i.e., thermal smoothing in the region ΔR between the optical absorption and pellet ablation surfaces.^{6,7} This mechanism effectively smooths out perturbations in the absorbed energy with transverse wavelength $\Lambda < \Delta R$.^{8,9} Unfortunately, the smoothing becomes less effective at shorter optical wavelengths because ΔR decreases with λ ;¹⁰ e.g., ΔR is typically $\sim 300 \mu\text{m}$ for $1 \mu\text{m}$ light, but only $\sim 50 \mu\text{m}$ for $\lambda = 1/4 \mu\text{m}$. For a high gain target of large size (a few mm radius) this small ΔR does not suffice.

Theoretical studies have shown that acceptable spherical illumination uniformity can be achieved by overlapping a limited number of beams (≥ 20), provided that each individual beam profile is smooth and reproducible.¹¹⁻¹³ However, previous efforts to obtain such profiles have been frustrated by the inherent imperfections in high power laser systems. The cumulative effect of small phase and amplitude aberrations (both linear and nonlinear) introduced by each optical element of a multistage laser is to produce large random nonuniformities in the output intensity. In order to produce the desired irradiance and spot size with a lens of reasonable focal length, one normally places the pellet in the quasi-

near-field of that lens, rather than at the focus; as a result, the laser nonuniformities tend to be mapped onto the pellet.^{12,14} Efforts to control laser aberrations, using ultra high quality optics and extensive beam relaying, have not been completely successful, especially at high energies and shorter laser wavelengths.¹⁵ Certain nonlinear optical techniques, such as phase conjugation¹⁶ and Raman beam smoothing,¹⁷⁻¹⁹ are capable of producing nearly diffraction-limited focal spots, but they do little to reduce the random low spatial frequency nonuniformities in the quasi near-field.^{18,20}

The Naval Research Laboratory has recently developed a simple technique called induced spatial incoherence (ISI), which allows a smooth and reproducible illumination profile at the pellet with modest quality laser beams.²¹⁻²³ The concept is illustrated in two dimensions in Fig. 1. Spatial incoherence is created by propagating a laser beam of broad bandwidth $\Delta\nu$ through an echelon structure that imposes different optical delays upon different transverse sections. By choosing the delay increments $t_{n+1} - t_n$ somewhat larger than the optical coherence time $t_c = 1/\Delta\nu$ (and the total time delay much smaller than the pulsewidth) one slices the beam into a large number of nearly simultaneous but incoherent beamlets, each of which focuses to the same smooth diffraction profile. Although superposition of these beamlets will produce a complicated interference pattern at any instant of time, that pattern evolves randomly in times of order t_c . The target surface will effectively ignore this rapidly shifting structure if the hydrodynamic response time t_h is much larger than t_c ; i.e., it responds only to the superposition of the intensity profiles. For example, a bandwidth $\Delta\nu = 30 \text{ cm}^{-1}$ will provide $t_c \approx 1 \text{ ps}$, whereas t_h is typically $\sim 1000 \text{ ps}$ for a high gain pellet.

The ISI concept is easily extended to three dimensions by using two perpendicular echelons constructed so that the time delay increment introduced by each step of one of them is slightly larger than the total delay increment across the other. Figure 2 illustrates this configuration, and Fig. 3 shows some recent experimental results with $1 \mu\text{m}$ light.²²

The diffraction profile is not very sensitive to intensity or phase aberrations on the incident beam; in fact, the beam need only be approximately uniform over the small width of each beamlet. Numerical simulations indicate that each echelon should have $N_s \geq 3N_{\text{ABER}}$ steps to adequately handle a beam aberrated to $N_{\text{ABER}} \times$ diffraction limit.²³

The ISI technique can thus provide the nearly uniform illumination needed to conduct realistic experimental studies of ablation physics at short wavelengths. In order to adequately test the reduction of Rayleigh-Taylor growth in a planar target geometry, these experiments will require an optical wavelength of $\sim 1/4 \mu\text{m}$ and a focal spot size of $500\text{-}600 \mu\text{m}$. The attainment of conditions relevant to laser fusion (e.g., intensities $\sim 3 \times 10^{14} \text{ W/cm}^2$ in a pulsewidth $\sim 5 \text{ ns}$) will then require on-target energies of $4\text{-}6 \text{ kJ}$, which will, in turn, require a $5\text{-}7 \text{ kJ}$ laser if one allows for $\sim 15\%$ losses in the ISI

and focusing optics. This laser must also operate with a bandwidth $\Delta\nu \sim 20\text{--}30\text{ cm}^{-1}$ and a beam quality better than $20 \times$ diffraction limit, in order to properly implement the ISI using echelons with a reasonable number of steps (e.g., $N_s \leq 50$). With the broadband capability, we will also be in a position to extend earlier NRL studies of the effects of bandwidth on plasma instabilities.²⁴

At the present time, the bandwidth requirement effectively rules out 4ω conversion from a large $1\text{ }\mu\text{m}$ glass laser, such as NOVA,²⁵ on account of the large UV dispersion in harmonic crystal materials. The possibility of using nonlinear optical techniques (e.g., nonlinear refraction²⁶ or rotational stimulated Raman scattering²⁷) to broaden the bandwidth after the harmonic conversion has taken place is under active consideration at NRL. Even if such techniques do prove to be feasible, however, they are likely to require an extensive development effort to avoid severe aberration in the output beam.

Our experimental requirements can be satisfied by an e-beam-pumped excimer laser, such as the AURORA KrF system^{28,29} currently under development at the Los Alamos National Laboratory (LANL). In this report, we will present the conceptual design of a smaller version of AURORA, with appropriate modifications for broadband operation and ISI. After a brief introduction to KrF laser fundamentals and the angular multiplexing technique, we will present a detailed baseline design of a 5-7 kJ system, along with discussion of related technical issues and problems. Finally, we will briefly consider an alternative design option using the Raman beam combination technique.

II. ANGULARLY MULTIPLEXED KrF LASERS

In the KrF laser, a mixture of Kr, Ar, and F_2 is pumped by an electrical discharge or e-beam to form several ionic and excited species, which combine to produce the short-lived KrF^* eximer.^{28,30,31} This eximer then dissociates to neutral Kr and F, plus the laser light around 248 nm. E-beam-pumped KrF can be scaled to large aperture, high energy operation without seriously degrading the optical beam quality.³¹ It is capable of attaining intrinsic efficiencies as high as 14%,^{32,33} which corresponds to an overall efficiency around 6-7%. The usable optical bandwidth of KrF is more than adequate for our needs. With a fluorescent linewidth $\Delta\nu_0 \approx 240\text{ cm}^{-1}$ FWHM ($\Delta\lambda \approx 1.5\text{ nm}$)³⁴ and an overall gain $G \approx 10^7$, a KrF oscillator-amplifier chain should provide gain-narrowed bandwidths up to $\Delta\nu_{\text{max}} \approx \Delta\nu_0 / (\ln G)^{1/2} \approx 60\text{ cm}^{-1}$.

Because the KrF^* lifetime is limited to a few nanoseconds by spontaneous radiative decay and collisional quenching,³¹ the KrF laser cannot be operated as an energy storage medium. Its energy must be extracted during the entire electrical pump pulse in order to attain optimum efficiency and avoid amplified spontaneous emission (ASE). (In a glass laser, by contrast, the upper level lifetime is $\sim 300\text{ }\mu\text{s}$; in that case, one can pump with a long flashlamp pulse, and still extract the stored energy in

nanosecond or subnanosecond optical pulses.) E-beam pulsewidths are generally required to be > 100 nsec in a large eximer system.³³ Shorter pulses are possible, but they result in severe cathode and foil loading at higher energies, and their risetimes are limited by the inductance in large cathode, switch, and bushing structures.

A short optical pulse can still be efficiently amplified in a nonstorage medium if one uses the angular multiplexing technique illustrated in Fig. 4.^{28,35-37} Using an optical encoding system, one first divides the pulse into several angular channels with differential time delays Δt . When these channels cross over one another at each amplifier stage, the light appears as a long continuous pulse. The separate channels are then re-synchronized (i.e., decoded) by an array of time-delay mirrors beyond the output stage, and the newly-coincident short pulses are combined at the target.

III. BASELINE DESIGN

Figure 5 shows the baseline design for a 48 beam system, which should be capable of producing a total $1/4 \mu\text{m}$ output energy of 5-7 kJ. At the input, a square 5 ns optical pulse is produced by a ~ 25 ns discharge-pumped oscillator/preamplifier, followed by one or more electro-optical shutters. This pulse is then spatially expanded and divided into 48 sequential channels by the temporal encoding optics, which consist of arrays of beam splitting and beam slicing mirrors spaced over suitable time delay paths. In the schematic, beam number 1 appears earliest, number 2 follows 5 ns later, etc. The 6×8 input feed-mirror array then directs the beams into the main laser chain so that they all cross at the e-beam-pumped preamplifier (20 cm) and intermediate amplifier (40 cm) modules. The output feed-mirror array performs a similar role for the 1 m large aperture module (LAM),^{28,29} which is double-passed to attain optimum energy extraction. After propagating over a sufficient distance (~ 90 m) to separate from one another, the beams are decoded by a combination of recollimator and time delay mirrors, as shown. Each of the 48 (approximately) coincident beams then propagates through its own ISI echelon pair and focusing lens, and the 48 incoherent focal spots overlap at the planar target. The recollimation, decoding, and target turning mirrors are conservatively designed for output energies ≤ 7 kJ, assuming a 1 J/cm^2 optical damage threshold and 2:1 peak/average intensity nonuniformities across each beam.

At this point, it is natural to ask whether it is really necessary to use the ISI technique; i.e., whether adequate beam smoothing would be provided by simple statistical averaging among the 48 beams. One answer is that even if the beam nonuniformities actually were random, the result of a 48 beam average would be marginal. The combined effects of Fresnel diffraction, off-axis aberrations, air turbulence, and e-beam deposition nonuniformities are likely to produce up to $\sim 50\%$ intensity varia-

tions across the quasi-near field output profiles. If these nonuniformities were truly random, then statistical averaging would reduce this by only $\sqrt{48}$ to about 7%. In fact, some of the nonuniformities, such as those arising from inhomogeneous e-beam deposition (typically $\pm 10\%$), are more likely to be systematic than random.

In order to build this system with minimal risk and delay, NRL proposes to use amplifier modules similar to those developed at LANL and Western Research Laboratories. The overall design is therefore similar to AURORA,^{28,29} with appropriate modifications to allow fewer beams, complete temporal decoding, and broadband operation with ISI. Table I shows a comparison of specifications for the two lasers.

A 48 channel multiplex with 5 ns optical pulses will require a 240 ns e-beam. The AURORA amplifier modules, however, are designed to operate at ~ 500 ns.^{28,29} This long pulse operation is dictated by a long e-beam risetime (> 100 ns) primarily due to high inductance in the bushing and switch sections (e.g., $H > 200$ nH in the LAM). If one simply shortened the electrical input pulse (by reducing the length of the water lines) without decreasing the risetime, it would result in significantly lower gain and output power. One solution to the problem would be to retain the full 500 ns e-beam, but use a 250 ns optical dump beam to load down the amplifiers (and thus suppress ASE) during the first half of it. The alternative approach proposed here is to lower the inductance by modifying the amplifier modules. Some specific modifications under considerations include (i) segmenting the cathode and feed lines,³⁸ (ii) use of rail switches and/or the NRL plasma switch,³⁹ and (iii) tapering of the rear wall of the cathode housing assembly to reduce the magnetic field volume.

Figure 6 shows one possible floor plan for the KrF laser. Note that the minimum allowable width of the building is determined by the length of the electrical water lines on the large aperture module. If the e-beam pulsewidth is reduced to 240 ns, the water lines would be shortened, as indicated, and the system could be compressed into a smaller building. The long, narrow duct containing the LAM-feed array, decoding optics, and ISI echelons must be carefully designed to minimize thermal gradients that could cause beam aberrations over the long air paths. An additional option under consideration is to overpressure this duct with an argon or other inert gas atmosphere to further reduce aberrations.

In the following paragraphs, each section of the laser will be examined in greater detail, and related technical issues, such as diffraction, dispersion, and beam quality, will be discussed.

A. Encoding Optics

Detailed views of the temporal encoding optics are shown in Figs. 7 and 8. In Fig. 7, a single 5 ns pulse incident from the right is divided by a combination of beam splitters and mirrors into four parallel

beams separated by 60 ns. Since these beams encounter no hard apertures and retain their initial 30 cm width, they experience little Fresnel diffraction in spite of the large distances over which they travel. The beams are then sliced by a combination of mirrors to produce the 6×8 array of sequential 6 cm, 5 ns pulses, as shown in Fig. 8. Here, the beams are much more susceptible to diffraction because of the hard aperture slicers and smaller widths.

This configuration was chosen to minimize Fresnel diffraction, which can produce intensity nonuniformities and crosstalk between adjacent channels (resulting in prepulses at the target). The fractional crosstalk due to diffractive coupling between adjacent parallel beams is approximately (Appendix A)

$$\epsilon \approx D/4\pi^2 N_F s, \quad (1)$$

where D is the beam width at the hard aperture, s is the spacing between the beams, and

$$N_F = D^2/\lambda z \quad (2)$$

is the Fresnel number at distance z from the aperture. In the above design, N_F is maximized by placing the slicers as close as possible to the input feed-mirror array (Fig. 5). This allows $z \leq 30$ m, $N_F \geq 480$ and $\epsilon \leq 2 \times 10^{-4}$ for $s = 1.5$ cm. In the usual encoder designs,^{28,29,37} in which the slicers appear first, the larger distance required ($z \leq 100$ m) would give only $N_F \geq 145$. The intensity profiles for the two options are compared in Fig. 9. Although this configuration admittedly requires more slicers than the conventional design, one should note that the extra slicers effectively replace the "scrambler" array³⁷ required in that design.

B. Amplifier Chain

Figure 10 shows a schematic side view of one of the edge beams propagating through the preamplifier and intermediate amplifier stages. Both this system and AURORA are designed so that all of the beams overlap and cross at the amplifier output lenses, which are imaged onto one another by the relay telescope. Here, the effective input pupil is defined by the preamplifier aperture, which is overfilled by about 20% to eliminate most of the Fresnel structure shown in Fig. 9b. Fresnel diffraction can start building up again after the intermediate amplifier, since there is no image relaying beyond this stage; however, this problem is mitigated by the large beam sizes. According to Appendix A, the Fresnel number for the 42 m path between the preamplifier ($D_0 = 40$ cm) and LAM-feed array mirrors ($D_1 = 8$ cm) is

$$(N_F)_1 = \frac{D_0 D_1}{\lambda z_{01}} = \frac{40 \times 8}{0.248 \times 10^{-4} \times 42 \times 100} = 3060. \quad (3)$$

Some care will be required to minimize both chromatic and off-axis aberrations in the amplifier chain. For a lens of focal length f , aperture D , and refractive index n , the chromatic aberration is given by (Appendix B)

$$N_{CA} = \frac{D^2 \lambda}{f} \frac{|\partial n / \partial \lambda|}{n-1} \Delta \nu, \quad (4)$$

where $\Delta \nu$ is the optical bandwidth in cm^{-1} . As an example, the 6 m telescope lens made of suprasil ($n \approx 1.5$, $\partial n / \partial \lambda = 5.6 \times 10^{-4} \text{ nm}^{-1}$) would give $N_{CA} \approx 15 \times$ diffraction limit for $\Delta \nu = 20 \text{ cm}^{-1}$.

The most serious off-axis aberration is astigmatism, whose contribution is given by (Appendix B)

$$N_{AST} = \frac{D^2 \theta^2}{f \lambda}, \quad (5)$$

where θ is the off-axis angle of the undeviated ray. In the worst case, $\theta \approx \pm 0.016$ for the edge beams at the 6 m telescope lens, thus giving $N_{AST} \approx 26 \times d.l.$ Although coma and spherical aberration can generally be minimized (at least within this portion of the optics) by appropriate lens design (Appendix B), the astigmatism will probably have to be compensated by other optical elements beyond this section. The choice of a single concave lens at the input of the 20 cm amplifier (instead of a relay telescope) was made in order to reduce both chromatic and off-axis aberrations.

Figure 11 shows a schematic top view of the two outer beams double-passing through the final amplifier (LAM) to the recollimator mirrors,^{36,37} which are arrayed in four steps separated by 75 cm (2.5 ns). As in the preceding amplifier stages, the beams overlap and cross at the LAM. The effective Fresnel numbers for the LAM-feed \rightarrow LAM and LAM \rightarrow recollimator sections are, respectively,

$$(N_F)_2 \approx \frac{8 \times 100}{0.248 \times 10^{-4} \times 43 \times 100} \approx 7470, \quad (6a)$$

$$(N_F)_3 \approx \frac{100 \times 18}{0.248 \times 10^{-4} \times 90 \times 100} \approx 8030. \quad (6b)$$

The off-axis feed geometry contributes to a significant amount of additional astigmatism and coma in the LAM mirror; in fact, expression (5) gives $N_{ABER} \approx 40 \times d.l.$ for the outermost beam ($\theta \approx 0.018$), due to astigmatism alone. The contribution due to coma is (Appendix B)

$$N_{COMA} = \frac{3pD^3 \theta}{16f^2 \lambda}, \quad (7)$$

where $p = 1 - 2f/s'$ and s' is the distance from the LAM mirror to the focal point beyond the collimators. In this case $s' \approx 111 \text{ m}$, so the coma contribution is $N_{COMA} \approx 5 \times d.l.$ for the outermost beam.

One could, in principle, compensate all of the astigmatism in each beam by adjusting the tilt angle of that beam's recollimator mirror, since $f < 0.36$. In practice, however, this approach would require the decoding mirrors to be distributed over an inordinately large region (both horizontally and vertically), and would limit the flexibility in dealing with any design modifications in the amplifier chain. Here, we propose a more flexible strategy; i.e., use the collimator mirrors to compensate that portion of the astigmatism that would result only from the off-axis LAM feed, thereby allowing the decoding mirrors to remain approximately in the horizontal plane. The remaining astigmatism would be compensated by tilting each target focusing lens around the axis normal to the effective sagittal plane for that beam.

An alternative recollimation scheme, as shown in Fig. 12, would replace the recollimator mirrors by an array of identical negative meniscus lenses. By tilting both these and the focusing lenses, one could compensate both astigmatism and residual coma in each beam, without the beam steering effects of the convex mirrors. The negative lenses would also provide partial compensation of chromatic aberration in the focusing lenses. Moreover, this scheme would completely separate the recollimators from the decoding optics, and thus allow greater flexibility in the design. We will pursue this point in greater detail in the following section.

C. Decoding Optics

Figure 13 gives a detailed view of the decoding optics, which clearly shows the difference in time delays imposed upon the earliest (1) and latest (48) channels. At the target aiming mirror array, all of these channels should be approximately synchronous, at least to within intervals short in comparison to the 5 ns pulsewidth. The figure also shows the larger offset angles of the outer beams (e.g., 21-24 and 45-48), which are used to partially compensate astigmatism from the LAM mirror, as discussed above.

For those beams that travel over the longest path, the Fresnel diffraction may be appreciable in this region. In the worst case (channel 1) the total optical path length between recollimator and target aiming mirrors is ≈ 100 m; thus, the Fresnel numbers satisfy the inequality

$$(N_F)_4 \geq \frac{(18)^2}{0.248 \times 10^{-4} \times 100 \times 100} \approx 1300. \quad (8)$$

The total diffraction in the path between the intermediate amplifier and target array is characterized by an effective Fresnel number (Appendix A)

$$(N_F)_{Total} = \left[(N_F)_1^{-1} + (N_F)_2^{-1} + (N_F)_3^{-1} + (N_F)_4^{-1} \right]^{-1} \geq 740, \quad (9)$$

which is still significantly better than that of the encoding optics.

If negative lenses were chosen instead of the mirror recollimators, as mentioned in the preceding section, it would provide the added advantage of greater flexibility in the decoding optics. For example, one could decode with only 48 isolated mirrors instead of the present configuration requiring two cross-linked sets of 48. This would be easier to align, and would probably be somewhat more stable; however, the overall cost is likely to be higher because (i) lenses are more expensive than mirrors of equal aperture, and (ii) one would lose the advantage of cross linking. (Each mirror would now require its own isolated frame.) The tradeoff between these two options will require further study.

D. ISI and Target Focusing Optics

Figure 14 shows a detailed view of the ISI and target focusing optics. Because the ISI echelons are placed in each of the 48 beams, they must be as simple and cheap as possible, and require minimal adjustment. These constraints dictate the use of transmissive optics in both the horizontal and vertical directions. With any reasonable number of steps, however, the echelons would have to be excessively thick along the propagation direction. The smallest differential step thickness must be at least $1/(n-1)\Delta\nu$, where n is the refractive index and $\Delta\nu$ is measured in cm^{-1} ; hence, for N_s steps, the larger echelon must have a thickness $z_{\text{max}} > N_s^2/(n-1)\Delta\nu$. Assuming $N_s = 40$, $n = 1.5$ and $\Delta\nu = 20 \text{ cm}^{-1}$, for example, one obtains $z_{\text{max}} > 1.6 \text{ m}$. An echelon of this thickness would not only be expensive and difficult to fabricate, but it could also cause a significant amount of self-focusing in the beamlets.

To avoid such problems, NRL proposes a partial ISI scheme, in which the step sequence would be repeated several times across the aperture,²³ as illustrated in the enlarged views in Fig. 14. Although this configuration allows repeated pairs of steps to remain mutually coherent, the resulting stationary interference pattern at the target will have a high spatial frequency $1/\lambda_T$, and can therefore be smoothed out by thermal diffusion^{6,7} in the plasma. In the example shown here, $\lambda_T = \lambda f/(10 \times 5 \text{ mm}) \sim 40 \mu\text{m}$ for $f = 8 \text{ m}$; hence, a plasma with an absorption-ablation distance $\Delta R = 50 \mu\text{m}$ will reduce the corresponding variation in the ablation pressure by roughly a factor of $\exp(-2\pi\Delta R/\lambda_T) \sim 4 \times 10^{-4}$. The relative variation (in comparison to the desired sinc^2 profile) is reduced by an additional factor of $(1/48)^{1/2}$ due to statistical averaging among the 48 beams.

Figures 15 and 16 compare the partial ISI scheme with the "pure" case discussed earlier. They show numerical simulations²³ of the time-averaged focal intensity distribution for an aberrated beam incident at the echelons, plus the average ablation pressure, assuming the heuristic thermal diffusion model discussed in the preceding paragraph. In both cases, a 20 cm, $5 \times$ diffraction limit beam (wavelength $\lambda = 0.527 \mu\text{m}$) is incident on the pair of echelons, each of which has a total of 20 1-cm wide steps. However, in the partial ISI scheme (Fig. 16) the sequence repeats after the 10th step; thus, steps 1 and 11, 2 and 12, etc. remain mutually coherent. The resulting increase in very fine-scale

interference structure is clearly evident at the focal plane, and would persist throughout the entire pulse duration. As a result of thermal smoothing, however, this structure is effectively filtered out. (The difference in peak/valley deviation in the two cases is purely statistical.) Note that the transverse wavelength $\lambda_T = 0.527 \mu\text{m} \times 600 \text{ cm} / (10 \times 1 \text{ cm}) \sim 32 \mu\text{m}$ due to the coherence is comparable to that of the KrF example.

The existence of a stationary intensity pattern, even one of high spatial frequency, raises the additional question of possible self-focusing in the underdense plasma. In order to examine this question, we have performed numerical simulations of optical propagation in the corona, using a cartesian 2D propagation/hydrodynamic code SELFOCT.²³ This code accounts for both ponderomotive and thermal self-focusing mechanisms, assuming linearized hydrodynamic response with strong ion-acoustic damping, and ignoring convection along the laser propagation axis. To compare the pure and partial ISI cases, we performed identical calculations using echelons with 40 steps. In the pure case, none of the steps were repeated, while in the partial case, two repeated sections of 20 steps were used. The plasma background was typical of a $1/4 \mu\text{m}$ laser-produced corona, with an electron temperature of 1.3 keV and a density scale length of $1275 \mu\text{m}$. The interaction was studied over a 0.5 cm path length in plasma densities varying between 1% and 50% critical. Although the simulation ran for times ≥ 640 ps (assuming a 3.17 ps coherence time) at average intensities of $3 \times 10^{14} \text{ W/cm}^2$, they showed no evidence of self-focusing in either case. Evidently, the averaged intensity distribution, even with the stationary nonuniformities introduced by the repeated steps, was below threshold for self-focusing.

Because the target is located at the focal point of the lenses, its intensity distribution is a sum over the far-field diffraction patterns of the echelon steps, and will therefore be independent of the distances between the echelons and lenses. In principle, then, one could replace the entire echelon array shown in Fig. 14 by a single pair of larger echelons located back at the LAM. (The step widths would be scaled up by the ratio 100 cm/18 cm.) This option is not recommended because it leads to excessive diffraction of the beamlets in the decoding optics. With Fresnel numbers of order unity, these beamlets would have peak intensities nearly three times the present value at some of the decoding mirrors. They would also be more susceptible to aberration due to thermal gradients in the long air paths, because their total widths (including low intensity "skirts" and sidelobes) are increased significantly by diffraction spreading.

E. Optical Alignment and Stability Requirements

Table II shows the mirror alignment precision and stability tolerances for the KrF system. With the exception of the target turning array, the alignment precision is required only to accurately center

the beam (within $\pm 5\%$) onto the next mirror in the laser chain. These alignment tolerances are within the resolution capabilities of the electronic control system currently under development on the AURORA laser.⁴⁰ The stability is required to maintain alignment throughout the chain, and to maintain the beam overlay at the target to within $15 \times$ diffraction limit (without the echelons). These tolerances are within state-of-the-art capabilities, and are comparable to those in the strip-mirror echelons used in the NRL Pharos III upgrade.

IV. RAMAN BEAM COMBINATION

In principle, it would be possible to significantly relax the alignment and stability tolerances and remove most of the aberration by using the Raman beam combination technique.¹⁷⁻¹⁹ This scheme could be implemented by crossing the output beams just beyond the target aiming mirror array at small angles θ to provide off-axis pumping radiation in a forward stimulated Raman amplifier. In order to allow a large aperture for this amplifier, one could either re-expand the beams (i.e., use convex mirrors in the aiming array) or group them into two or more crossed clusters of closely-spaced parallel beams. (For example, three 4×4 clusters would provide a minimum effective pumping aperture ≥ 80 cm.) The Stokes "seed" beam would be generated in a Raman oscillator, spatially filtered to ensure good beam quality, and directed along the axis of the Raman amplifier cell. In the case of narrowband light, both theory^{17,19} and experiment¹⁷⁻¹⁹ have shown that the Stokes beam can efficiently extract the pump energy without picking up much of the spatial structure due to aberration provided that (i) the effective diffraction lengths $l_D = \lambda/\pi\theta^2$ are short in comparison to the gain e-folding distances, and (ii) none of the pump beams have any appreciable components along the axis.

Unfortunately, it does not appear to be practical to implement this technique using the broadband light required for ISI. Orlov, et al.⁴¹ have shown that the Stokes beam will pick up the aberrated pump beam structure if the broadband pump radiation is spatially incoherent. More recent calculations performed at NRL indicate that the amplified Stokes light can still maintain good beam quality, even with broadband operation, if one satisfies the additional criteria that (iii) the seed beam is precorrelated with one of the pump beams, and (iv) the Stokes and all of the pump beams remain mutually coherent across the aperture of the Raman cell. The first condition is relatively easy to satisfy, since one of the KrF beams would presumably also be used to pump the Raman oscillator. For the bandwidths of interest here, however, the second condition would not only require all of the incident pump beams to be synchronized to within $ct_c = 1/\Delta\nu < \frac{1}{2}$ mm, but would also place a severe constraint upon the maximum allowable beam crossing angle θ_{\max} :

$$D \tan\theta_{\max} < 1/\Delta\nu, \quad (10)$$

where D is the effective aperture of the Raman cell. For a bandwidth $\Delta\nu = 20 \text{ cm}^{-1}$ and $D = 1 \text{ m}$, expression (10) would require $\theta_{\text{max}} < \frac{1}{2} \text{ mrad}$, which would in turn require a distance of approximately 2 km between the aiming mirrors and Raman cell.

V. SUMMARY, MANAGEMENT, AND SCHEDULE

As a first step in providing the $1/4 \mu\text{m}$ irradiation needed for future planar target ablation experiments, NRL has completed the baseline design of a 48 beam angularly multiplexed KrF laser based on AURORA-type amplifier modules. This system is designed for broadband operation ($20\text{-}30 \text{ cm}^{-1}$) with induced spatial incoherence (40-50 steps/echelon in each beam) at the focusing optics, and should provide on-target energies of 4-6 kJ in a 5 ns pulse. Although the off-axis forward Raman beam combination technique offers the promise of improved beam quality and less stringent alignment and stability tolerances, it does not appear practical for this system on account of the wide bandwidths that are required.

Table III shows a cost estimate of the system, including the building and target facility. The Naval Research Laboratory will serve as prime contractor for the project. We are currently planning to divide the work into seven components: (1) large aperture modules, (2) optics with mounts and alignment hardware, (3) building, (4) chamber system, (5) oscillator, (6) I.S.I. array, and (7) control system. Each component would have separate contracts for detailed design, construction and installation. Contractors could bid on one or more of these components.

The first twelve months (FY 86) would primarily be devoted to finalizing the details of the baseline design in each of the seven areas. We would also start development of the oscillator and the ISI arrays. Total expenditures are estimated at \$2-3M.

In the second twelve months, (FY 87) we would let contracts to procure most of the seven components. Total expenditures are estimated at \$16M. If the building is at the 30% design level by the end of CY 85 it could be funded in the FY 87 budget. Construction time is estimated at 10 months.

In the third year (FY 88) construction would end, components tested, and installation begun. Total expenditures are estimated at \$2M, plus \$4M operating costs.

After the construction has ended, routine operating costs are estimated at \$6.5M/year. (This is an increase of \$3.5M over the current NRL program.) Routine operation on target would begin in late FY89.

Appendix A

FRESNEL DIFFRACTION FROM A SQUARE APERTURE

Consider a light wave of complex amplitude $E(\bar{r}_0, 0) = E(x_0, y_0, 0)$ with beam curvature $R_0 (> 0$ if converging) traversing a square aperture of width D_0 located at plane $z = 0$ (Fig. 17). In general, one can write

$$E(\bar{r}_0, 0) = E_C(\bar{r}_0, 0) \exp(-ik|\bar{r}_0|^2/2R_0),$$

where $E_C(\bar{r}, 0)$ is the collimated version of $E(\bar{r}_0, 0)$, $k = 2\pi/\lambda$, and the exponential accounts for the beam curvature. At plane z_1 , the amplitude is given by the Fresnel diffraction integral⁴²

$$E(\bar{r}_1, z_1) = \frac{1}{i\lambda z_1} \int_{-\frac{1}{2}D_0}^{\frac{1}{2}D_0} dx_0 \int_{-\frac{1}{2}D_0}^{\frac{1}{2}D_0} dy_0 E_C(\bar{r}_0, 0) \exp\left[\frac{ik}{2} \left(\frac{|\bar{r}_0 - \bar{r}_1|^2}{z_{01}} - \frac{|\bar{r}_0|^2}{R_0} \right)\right] \quad (\text{A1})$$

$$= M_{01} E_C(M_{01}\bar{r}_1, M_{01}z_{01}) \exp(-ik|\bar{r}_1|^2/2R_1), \quad (\text{A2})$$

where $R_1 = R_0 - z_{01} = R_0 - z_1$,

$$M_{01} \equiv R_0/z_1 = D_0/D_1 \quad (\text{A3})$$

is a geometrical-optics magnification factor (see Fig. 17), and

$$E_C(\bar{r}, z) \equiv \frac{1}{i\lambda z} \int_{-\frac{1}{2}D_0}^{\frac{1}{2}D_0} dx_0 \int_{-\frac{1}{2}D_0}^{\frac{1}{2}D_0} dy_0 E_C(\bar{r}_0, 0) \exp\left[\frac{ik}{2} \frac{|\bar{r}_0 - \bar{r}|^2}{z}\right] \quad (\text{A4})$$

describes the diffraction of a collimated beam propagating over distance z . The diffraction of a beam of arbitrary curvature can thus be related to that of collimated light by a simple procedure: (i) remove the geometrical curvature from the incident wave, (ii) propagate the resulting collimated wave to the new plane, scaling both the distance and new transverse coordinates by the appropriate magnification factor. (iii) rescale the amplitude and reinstate the new geometrical curvature.

If a lens (or curved mirror) is now placed at z_1 , the beam will acquire a new curvature R'_1 . The amplitude at plane z_2 at distance $z_{12} = z_2 - z_1$ will then be given by

$$E(\bar{r}_2, z_2) = \frac{M_{01}}{i\lambda z_{12}} \int dx_1 \int dy_1 E_C(M_{01}\bar{r}_1, M_{01}z_{01}) \exp\left[\frac{ik}{2} \left(\frac{|\bar{r}_1 - \bar{r}_2|^2}{z_{12}} - \frac{|\bar{r}_1|^2}{R'_1} \right)\right].$$

If one multiplies and divides the exponential argument by M_{01}^2 and changes the integration variable to $M_{01}\bar{r}_1$, then this expression will have the same form as Eq. (A1); hence one can immediately write

$$E(\bar{r}_2, z_2) = M_{01}M_{12}E_C(M_{01}M_{12}\bar{r}_2, M_{01}z_{01} + M_{01}^2M_{12}z_{12}) \exp(-ik|\bar{r}_2|^2/2R_2), \quad (\text{A5})$$

where $R_2 = R_1 - z_{12}$ and

$$M_{12} = R_1/R_2 = D_1/D_2. \quad (\text{A6})$$

The beam "width" D_2 is again defined by the geometrical-optics ray paths, just as D_1 was defined in Eq. (A3). Thus

$$M_{01}M_{12} = D_0/D_2 \equiv M_{02}$$

as one might expect from the functional form of (A5). If the lens is removed from the z_1 plane, then $R_1 \rightarrow R_1$ and $M_{01}z_{01} + M_{01}^2M_{12}z_{12} \rightarrow M_{02}z_{02}$; therefore, (A5) reduces the (A2) with $M_{01} \rightarrow M_{02}$, $\bar{r}_1 \rightarrow \bar{r}_2$, $z_{01} \rightarrow z_{02}$, and $R_1 \rightarrow R_2$.

We now apply these results to the case where the aperture at $z = 0$ is uniformly illuminated. Then $E_C(\bar{r}_0, 0) \equiv E_0$ is constant, and Eq. (A4) factorizes into

$$E_C(\bar{r}, z) = A(x, z) A(y, z). \quad (\text{A7})$$

Here,

$$A(x, z) \equiv \left(\frac{E_0}{i\lambda z} \right)^{1/2} \int_{-\frac{1}{2}D_0}^{\frac{1}{2}D_0} dx_0 \exp \left[\frac{ik}{2} \frac{(x_0 - x)^2}{z} \right] - \left(\frac{E_0}{2i} \right)^{1/2} \left\{ F \left[\left(\frac{1}{2}N_F \right)^{1/2} (2x/D_0 + 1) \right] - F \left[\left(\frac{1}{2}N_F \right)^{1/2} (2x/D_0 - 1) \right] \right\}, \quad (\text{A8})$$

$$F(W) \equiv \int_0^W \exp \left[i \frac{\pi}{2} W'^2 \right] dW' = -F(-W) \quad (\text{A9})$$

is the Fresnel integral, and

$$N_F \equiv D_0^2/\lambda z \quad (\text{A10})$$

is the Fresnel number for a collimated beam. Substituting these results into expression (A2), one obtains for the intensity at z_1

$$|E(\bar{r}_1, z_1)|^2 = M_{01}^2 |A(M_{01}x_1, M_{01}z_{01})|^2 |A(M_{01}y_1, M_{01}z_{01})|^2, \quad (\text{A11})$$

where according to definition (A3),

$$A(M_{01}x_1, M_{01}z_1) = \left(\frac{E_0}{2i}\right)^{1/2} \left\{ F\left[\left(\frac{1}{2}N_{01}\right)^{1/2} (2x_1/D_1 + 1)\right] - F\left[\left(\frac{1}{2}N_{01}\right)^{1/2} (2x_1/D_1 - 1)\right] \right\}, \quad (\text{A12})$$

and

$$N_{01} \equiv D_0^2/\lambda M_{01}z_{01} = D_0 D_1/\lambda z_{01} \quad (\text{A13})$$

is the effective Fresnel number of the converging or diverging beam. Expression (A12) thus has the same functional form as (A8), with appropriate changes in the transverse scaling and the Fresnel number. Similar considerations apply to Eq. (A5):

$$\begin{aligned} |E(\vec{r}_2, z_2)|^2 &= M_{01}^2 M_{12}^2 |A(M_{01}M_{12}x_2, M_{01}z_{01} + M_{01}^2 M_{12}z_{12})|^2 \\ &\times |A(M_{01}M_{02}x_2, M_{01}z_{01} + M_{01}^2 M_{12}z_{12})|^2. \end{aligned}$$

Combining Eqs. (A8), (A10), (A3) and (A6), one obtains the expression for $A(M_{01}M_{12}x_2, M_{01}z_{01} + M_{01}^2 M_{12}z_{12})$ identical to Eq. (A12) with $x_1 \rightarrow x_2$, $D_1 \rightarrow D_2$, and $N_{01} \rightarrow N_{02}$ defined by

$$N_{02} \equiv \frac{D_0^2}{\lambda M_{01}z_{01} + M_{01}^2 M_{12}z_{12}} = (N_{01}^{-1} + N_{12}^{-1})^{-1}, \quad (\text{A14})$$

$$N_{12} \equiv D_1 D_2/\lambda z_{12}. \quad (\text{A15})$$

We now use these results to estimate the fractional energy ϵ diffracted into the shadow zone $x > \frac{1}{2}D_0$ on one side of the beam. For simplicity, consider the collimated case, and define the distance $s \equiv x - \frac{1}{2}D_0$ into the shadow zone. Expression (A8) can then be written as

$$A(x, z) = \left(\frac{E_0}{2i}\right)^{1/2} \{ F[(2N_F)^{1/2}(s/D_0 + 1)] - F[(2N_F)^{1/2}s/D_0] \}.$$

In the cases of interest, where $N_F^{1/2} \gg 1$, both arguments of $F(W)$ can satisfy $W > 1$ even for $x \geq D_0/2$; hence, one can approximate (A9) by its asymptotic form for $W \gg 1$, giving

$$A(x, z) \approx \frac{(iE_0)^{1/2}}{2\pi N_F^{1/2}} \left\{ \frac{\exp[i\pi N_F(s/D_0)^2]}{s/D_0} - \frac{\exp[i\pi N_F(s/D_0 + 1)^2]}{s/D_0 + 1} \right\}.$$

For points $|y| < \frac{1}{2}D_0$, the shadow zone intensity is approximately

$$\begin{aligned}
 |E_C(x, 0, z)|^2 &= |A(x, z)|^2 |E_0| \\
 &\approx \frac{|E_0|^2 D_0^2}{4N_F} \left\{ \frac{1}{s^2} + \frac{1}{(s + D_0)^2} - \frac{2}{s(s + D_0)} \cos[\pi N_F (2s/D_0 + 1)] \right\}.
 \end{aligned} \tag{A16}$$

The fractional energy diffracted to all points $s' \geq s$ is then

$$\begin{aligned}
 \epsilon &= \frac{1}{|E_0|^2 D_0^2} \int_s^\infty |E_C(x', 0, z)|^2 D_0 ds' \\
 &\approx \frac{D_0}{4\pi^2 N_F s} \left(1 + \frac{s}{s + D_0} \right) \approx \frac{D_0}{4\pi^2 N_F s},
 \end{aligned} \tag{A17}$$

where the rapidly-varying contribution due to the cosine term of (A16) has been ignored.

Appendix B

PRIMARY ABERRATIONS OF SPHERICAL MIRRORS AND LENSES

This appendix examines the increase in focal spot size due to (i) primary Seidel aberrations⁴² of spherical mirrors and thin lenses, and (ii) on-axis chromatic aberration in thin lenses. Figure 18 shows a spherical mirror of radius $R = 2f$, which is illuminated by an object point P located at axial distance s and height h . Point P' is defined as the image point in the paraxial ray approximation; i.e., the relations

$$h/s = h'/s' = \tan\theta \quad (\text{B1})$$

$$1/s + 1/s' = 1/f = 2/R \quad (\text{B2})$$

are satisfied identically. The aberration of a ray striking the spherical mirror surface at point $Q = Q(r, \phi)$ is then defined by the difference

$$\delta_s \equiv \overline{PQ} + \overline{QP'} - \overline{PO} - \overline{OP'} \quad (\text{B3})$$

between the virtual optic path $\overline{PQP'}$ and the real (i.e., undeviated) path $\overline{POP'}$. In terms of the polar coordinates (α, ϕ) ,

$$\overline{PQ} = [(h - R \sin\alpha \cos\phi)^2 + (R \sin\alpha \sin\phi)^2 + (R - R \cos\alpha - s)^2]^{1/2},$$

$$\overline{QP'} = [(h' + R \sin\alpha \cos\phi)^2 + (R \sin\alpha \sin\phi)^2 + (R - R \cos\alpha - s')^2]^{1/2},$$

$$\overline{PO} = (s^2 + h^2)^{1/2}, \quad \overline{OP'} = (s'^2 + h'^2)^{1/2}.$$

Substituting these expressions into (B3), using Eqs. (B1) and (B2) to eliminate h and s , and expanding up to fourth order in the small quantities h' and $r \equiv R\alpha$, one obtains the optical path difference

$$\delta_s = -\frac{1}{4}Br^4 + Fr^3\cos\phi \tan\theta - Cr^2\cos^2\phi \tan^2\theta. \quad (\text{B4})$$

The Seidel aberration coefficients are.

$$B = p^2/8f^3 \quad (\text{Spherical Aberration}) \quad (\text{B5})$$

$$F = p/4f^2 \quad (\text{Coma}) \quad (\text{B6})$$

$$C = 1/2f \quad (\text{Astigmatism}), \quad (\text{B7})$$

where $p \equiv 1 - 2f/s$. For a thin spherical lens of refractive index n , one again obtains expression (B4) [plus a field curvature term $-\frac{1}{2}Dr^2\tan^2\theta$] with coma and spherical aberration coefficients that depend on the shape factor

$$q = \frac{1/R_1 + 1/R_2}{1/R_1 - 1/R_2},$$

where $R_1(R_2)$ is the curvature of the left (right)-hand surface.⁴² The astigmatism coefficient is identical to Eq. (B7), and the curvature term is

$$D = (1/2f)(n + 1)/n.$$

In the paraxial ray approximation, the optical delay path in a lens is $T - r^2/2f$, where T is a constant. The optical path difference resulting from chromatic aberration is then

$$\delta_c = -\frac{\partial(1/f)}{\partial\lambda} \Delta\lambda \frac{r^2}{2} = \frac{\partial(1/f)}{\partial\lambda} \lambda^2 \Delta\nu \frac{r^2}{2}, \quad (\text{B8})$$

where $\Delta\nu$ is the laser bandwidth in cm^{-1} . Substituting the expression

$$1/f = (n - 1)(1/R_1 - 1/R_2) \quad (\text{B9})$$

for the paraxial focal length, one obtains

$$\delta_c = \frac{\partial n/\partial\lambda}{n - 1} \lambda^2 \Delta\nu \frac{r^2}{2f}. \quad (\text{B10})$$

One can now derive simple expressions for the increase in focal spot size

$$d_{\text{ABER}} = f \left| (\nabla_{\perp} \delta)_{\text{MAX}} - (\nabla_{\perp} \delta)_{\text{MIN}} \right| \quad (\text{B11})$$

that would result from each of these aberrations. (∇_{\perp} is the transverse gradient.) In comparison to the diffraction-limited width $d_{DL} = f\lambda/D$ (where D is the width of the beam at the lens) the broadening due to aberration is

$$N_{\text{ABER}} = d_{\text{ABER}}/d_{\text{DL}} \approx (D/\lambda) \left[(\nabla_{\perp} \delta)_{\text{MAX}} - (\nabla_{\perp} \delta)_{\text{MIN}} \right]. \quad (\text{B12})$$

Spherical aberration: Expression (B4) gives $(\nabla_{\perp} \delta)_{\text{MAX}} = B(\frac{1}{2}D)^3 = -(\nabla_{\perp} \delta)_{\text{MIN}}$; hence, for a spherical mirror,

$$N_{\text{ABER}} \rightarrow N_{\text{SA}} = \frac{p^2 D^4}{32 f \lambda}. \quad (\text{B13})$$

Coma: $(\nabla_{\perp} \delta)_{\text{MAX}} = 3F(\frac{1}{2}D)^2 \theta$ (assuming $\theta \ll 1$) and $(\nabla_{\perp} \delta)_{\text{MIN}} = 0$; hence, for a spherical mirror,

$$N_{\text{ABER}} \rightarrow N_{\text{COMA}} = \frac{3pD^3\theta}{16f^2\lambda}. \quad (\text{B14})$$

Astigmatism: $(\nabla_{\perp} \delta)_{\text{MAX}} = 2C\frac{1}{2}D\theta^2 = -(\nabla_{\perp} \delta)_{\text{MIN}}$; hence, for either a spherical mirror or thin lens

$$N_{\text{ABER}} \rightarrow N_{\text{AST}} = \frac{D^2\theta^2}{f\lambda}. \quad (\text{B15})$$

Chromatic aberration: Substituting Eq. (B10) into (B12), and calculating the maximum and minimum values as above, one obtains

$$N_{\text{ABER}} \rightarrow N_{\text{CA}} = \frac{D^2\lambda}{f} \frac{|\partial n/\partial \lambda|}{n-1} \Delta\nu. \quad (\text{B16})$$

REFERENCES

1. C. Garban-Labaune, E. Fabre, C.E. Max, R. Fabbro, F. Amiranoff, J. Virmont, W. Weinfeld, and A. Michard, *Phys. Rev. Lett.* **48**, 1018 (1982); W. Seka, R.S. Craxton, J. Delettrez, L. Goldman, R. Keck, R.L. McCrory, D. Shvarts, J.M. Soures, and R. Boni, *Opt. Commun.* **40**, 437 (1982).
2. D.C. Slater, G.E. Busch, G. Charatis, R.R. Johnson, F.J. Mayer, R.J. Schroeder, J.D. Simpson, D. Sullivan, J.A. Tarvin, and C.E. Thomas, *Phys. Rev. Lett.* **46**, 1199 (1981); W.C. Mead, E.M. Campbell, K.G. Estabrook, R.E. Turner, W.L. Kruer, P.H.Y. Lee, B. Pruett, V.C. Rupert, K.G. Tirsell, G.L. Stradling, F. Ze, C.E. Max, and M.D. Rosen, *Phys. Rev. Lett.* **47**, 1289 (1981); M.C. Richardson, R.S. Craxton, J. Delettrez, R.L. Keck, R.L. McCrory, W. Seka, and J.M. Soures, *Phys. Rev. Lett.* **54**, 1656 (1985); C. Garban-Labaune, E. Fabre, C. Max, F. Amiranoff, R. Fabbro, J. Virmont, and W.C. Mead, *Phys. Fluids* **28**, 2580 (1985).
3. C.E. Max and K.G. Estabrook, *Comments Plasma Phys. Cont. Fusion* **5**, 239 (1980).
4. S. Bodner, W. Emery, J. Gardner, J. Grun, M. Herbst, S. Kacenjar, R. Lehmborg, C. Manka, E. McLean, S. Obenschain, B. Ripin, A. Schmitt, J. Stamper, and F. Young, *IAEA 10th International Conference on Plasma Physics and Controlled Nuclear Fusion Research (London, U.K., 12-19 Sept. 1984) IAEA-CN-44*.
5. M.H. Emery, *Bull. Am. Phys. Soc.* **29**, 1231 (1984).
6. S.E. Bodner, *J. Fusion Energy* **1**, 221 (1981); "Laser Interaction and Related Plasma Phenomena," Vol. 6, Edited by Heinrich Hora and G.H. Miley (Plenum Press, 1984).
7. J. Nuckolls, L. Wood, A. Thiessen, and G. Zimmerman, *Nature* **239**, 15 Sept, 139 (1972).
8. M.H. Emery, J.H. Gardner, J.P. Boris, and J. H. Orens, *Naval Research Laboratory Memorandum Report 4500* (1981); *Phys. Rev. Lett.* **48**, 253 (1982).
9. S.P. Obenschain, J. Grun, B.H. Ripin, and E.A. McLean, *Phys. Rev. Lett.* **46**, 1402 (1981); S.P. Obenschain, R.R. Whitlock, E.A. McLean, B.H. Ripin, R.A. Price, D.W. Phillion, E.M. Campbell, M.D. Rosen, and J.M. Auerbach, *Phys. Rev. Lett.* **50**, 44 (1983).
10. J.H. Gardner and S.E. Bodner, *Phys. Rev. Lett.* **47**, 1137 (1981).

11. J.E. Howard, *Appl. Opt.* **16**, 2764 (1977).
12. S. Skupsky and K. Lee, *J. Appl. Phys.* **54**, 3662 (1983).
13. A.J. Schmitt, *Appl. Phys. Lett.* **44**, 399 (1984).
14. J.M. McMahon, R.P. Burns, T.H. DeRieux, R.A. Hunsicker, and R.H. Lehmberg, *IEEE J. Quantum Electron.* **QE-17**, 1629 (1981).
15. University of Rochester Laboratory for Laser Energetics Annual Report (1 October 1983 – 30 September 1984) ed. by R.L. McCrory; M.C. Richardson, et al., Digest of the 1985 Conference on Lasers and Electro-Optics (Baltimore, MD, 21-24 May 1985) paper THS1
16. B. Ya. Zel'dovich, N.F. Pilipetsky, and V.V. Shkunov, "Principles of Phase Conjugation" (Springer-Verlag, 1985)
17. J. Goldhar and J.R. Murray, *IEEE J. Quantum Electron.* **QE-18**, 399 (1982).
18. J. Goldhar, M.W. Taylor, and J.R. Murray, *IEEE J. Quantum Electron.* **QE-20**, 772 (1984).
19. R.S.F. Chang, R.H. Lehmberg, M.T. Duignan, and N. Djeu, *IEEE J. Quantum Electron.* **QE-21**, 477 (1985).
20. R.H. Lehmberg, *Opt. Commun.* **43**, 369 (1982); *J. Opt. Soc. Am.* **73**, 558 (1983).
21. R.H. Lehmberg and S.P. Obenschain, *Opt. Commun.* **46**, 27 (1983).
22. S.P. Obenschain, J. Grun, M. J. Herbst, K.J. Kearney, C.K. Manka, J.A. Stamper, R.A. Hunsicker, S. Kacenjar, R.H. Lehmberg, E.A. McLean, M. Pronko, and F.C. Young, *Bull. Am. Phys. Soc.* **29**, 1184 (1984).
23. R.H. Lehmberg, S.P. Obenschain, and A.J. Schmitt, *Bull. Am. Phys. Soc.* **29**, 1184 (1984).
24. M.J. Herbst, C.K. Manka, S.P. Obenschain, K.J. Kearney, and F.C. Young, *Bull. Am. Phys. Soc.* **29**, 1183 (1984).
25. D.R. Speck, R.O. Godwin, and W.W. Simmons, Digest of the 1985 Conference on Lasers and Electro-Optics (Baltimore, MD, 21-24 May 1985) paper THY1
26. J.F. Reintjes, "Nonlinear Optical Parametric Processes in Liquids and Gases" (Academic Press, 1984) Sec. 4.3.

27. D. Eimerl and J.R. Murray, Lawrence Livermore National Laboratory 1979 Annual Report (Laser Program, Vol. 3) UCRL-50021-79 (1980), p. 7-64; G.E. Busch, Digest of the 1981 Conference on Lasers and Electro-Optics (Washington, D.C., 10-12 June 1981). paper THB13
28. R.J. Jensen, Summary of Research for the ICF Program at Los Alamos National Laboratory, LA-10380 (March 1985) p. 23.
29. L.A. Rosocha, Digest of the 1985 Conference on Lasers and Electro-Optics (Baltimore, MD, 21-24 May 1985) paper THL2.
30. T.H. Johnson and A.M. Hunter, II, J. Appl. Phys. 51, 2406 (1980).
31. M. Rokni and J.H. Jacob, "Applied Atomic Collision Physics," Vol. 3, ed. by E.W. McDaniel and W.L. Nighan (Academic press, 1982) Chapter 10.
32. W.D. Kimura and E.T. Salesky, Digest of the 1985 Conference on Lasers and Electro-Optics (Baltimore, MD, 21-24 May 1985) paper THF1; A. Mandl, D. Klimek, and E.T. Salesky, *ibid.* paper THF2.
33. C.W. von Rosenberg, Jr., D.E. Klimek, and J.H. Jacob, IAEA 10th International Conference on Plasma Physics and Controlled Nuclear Fusion Research (London, U.K., 12-19 Sept. 1984) IAEA-CN-44.
34. J.R. Murray, J. Goldhar, and A. Szoke, Lawrence Livermore National Laboratory 1977 Annual Report (Laser Program, Vol. 2) UCRL-50021-77 (1978) p7-94.
35. J.J. Ewing, R.A. Haas, J.C. Swingle, E.V. George, and W.F. Krupke, IEEE J. Quantum Electron. QE-15, 368 (1979).
36. D. Eimerl, J. Goldhar, R.R. Jacobs, J.R. Murray, W.R. Rapoport, L.G. Schlitt, and J.C. Swingle, Lawrence Livermore National Laboratory 1979 Annual Report (Laser Program, Vol. 3) UCRL-50021-79 (1980) p. 7-21; R.A. Haas and L.G. Seppala, *ibid.* p 7-40.
37. A.M. Hunter, II, R.O. Hunter, and T.H. Johnson, IEEE J. Quantum Electron. (in press) (1985).
38. D.A. Reilly and C.W. von Rosenberg, Digest of the 1985 Conference on Lasers and Electro-Optics (Baltimore, MD 21-24 May 1985) paper THF4.
39. R.A. Meger, R.J. Commisso, G. Cooperstein, and S.A. Goldstein, Appl. Phys. Lett. 42, 943 (1983).

40. B.L. Kortegaard, SPIE Technical Symposium on Optical and Electro-Optical Engineering (Los Angeles, CA, 23-25 Jan. 1985).
41. V.K. Orlov, V.B. Gerasimova, S.A. Gerasimova, and E.M. Zemskov, Sov. J. Quantum Electron. 7-79 (1977).
42. M. Born and E. Wolf, "Principles of Optics" (Pergamon Press, 1964).

Table 1

**COMPARISON OF PROPOSED KrF LASER TO
LANL/WESTERN RESEARCH AURORA SYSTEM**

	AURORA	PROPOSED NRL SYSTEM
OUTPUT ENERGY	10-15 kJ	5-7 kJ
NUMBER OF BEAMS	96	48
ELECTRICAL PULSEWIDTH	500 ns	~ 250 ns
OPTICAL OUTPUT PULSEWIDTH	MOST OF ENERGY IN 500 ns	5 ns
MULTIPLEXING	ALL BEAMS ENCODED, < 25 BEAMS DECODED	ALL 48 BEAMS ENCODED AND DECODED
BANDWIDTH	> 20 cm ⁻¹	> 20 cm ⁻¹
BEAM QUALITY	EMPHASIS ON RADIATION-DRIVEN TARGETS	N _{ABER} < 20

Table II

ALIGNMENT AND STABILITY REQUIREMENTS

MIRRORS	NUMBER OF ELEMENTS	ALIGNMENT PRECISION (μrad)	STABILITY (μrad)
30 cm ENCODERS	6	150-800	10-25
BEAM SLICERS	64	125	33
INPUT-FEED ARRAY	48	170	33
LAM-FEED ARRAY	48	500	6
LAM-MIRROR	1	50	6
RECOLLINATORS/DECODERS	96	90	10
TARGET TURNING ARRAY	48	10	10

Table III

COST ESTIMATES
48 BEAM KrF LASER AND TARGET FACILITY

	\$(THOUSANDS)
OSCILLATOR AND PULSE SHAPING	700
AMPLIFIERS	2100
MECHANICAL HARDWARE	1600
OPTICS	2900
I.S.I. ECHELONS	2000
TARGET FACILITY	2000
ENGINEERING AND ASSEMBLY	3000
BUILDING	3500
CONTINGENCY (R&D)	2200
	\$20M

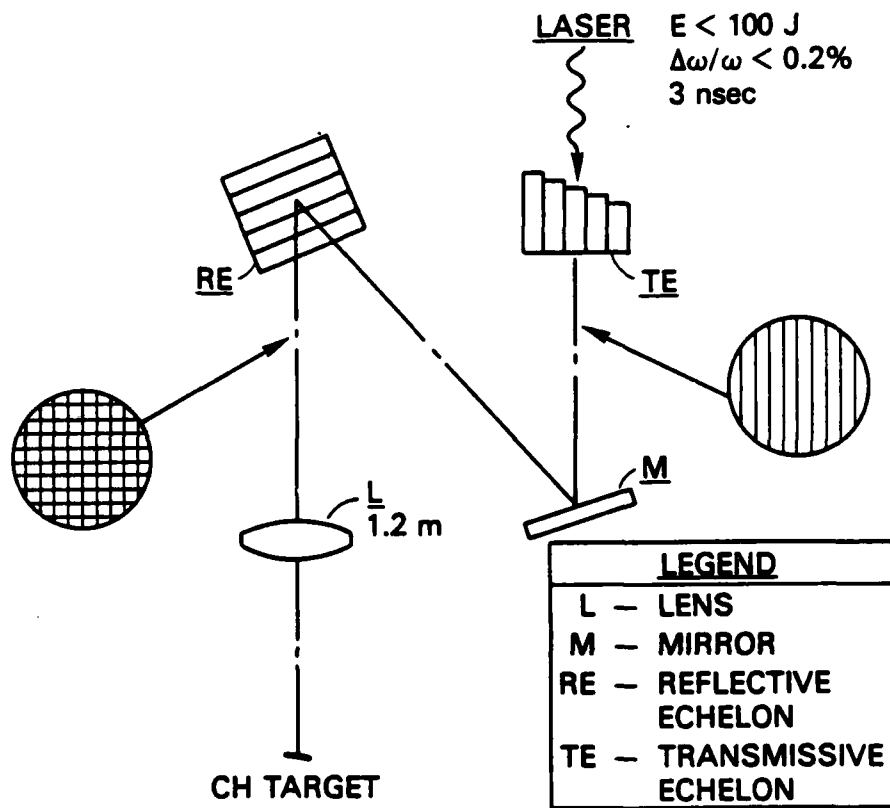
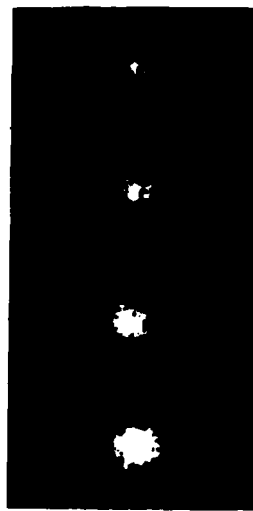


Fig. 2 - Experimental configuration for induced spatial incoherence (ISI) using one reflecting and one transmitting echelon, and an F/6 lens

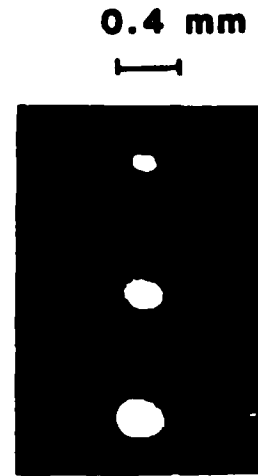
(0.5x Contours)



PLAIN LASER



**WITH ECHELONS
NARROWBAND**



**WITH ECHELONS
WIDEBAND**

Fig. 3 - Focal distribution observed with and without the ISI. (Iso-intensity contours, with each spot 1/2 the intensity of the one above it.)

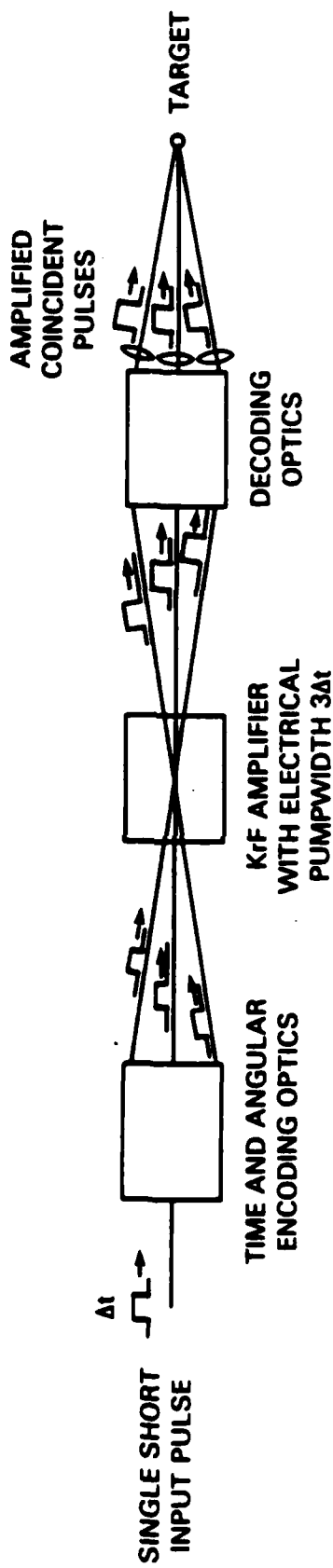


Fig. 4 — Illustration of the angular multiplexing technique to achieve efficient amplification of a short optical pulse in a laser amplifier with long pulse excitation

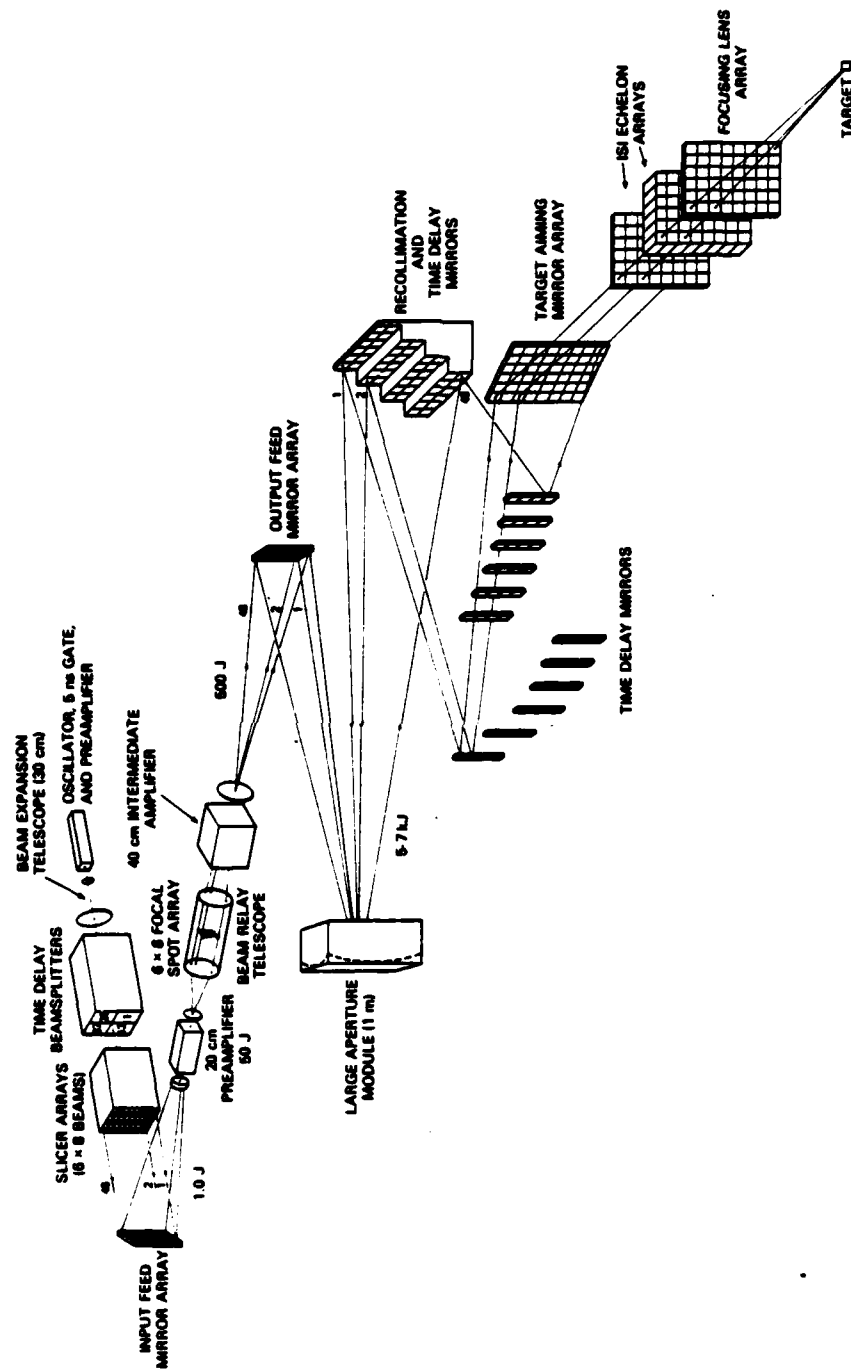


Fig. 5 — Proposed baseline design of a 5-10 kJ angularly multiplexed KrF laser, with ISI in each of the 48 output beams

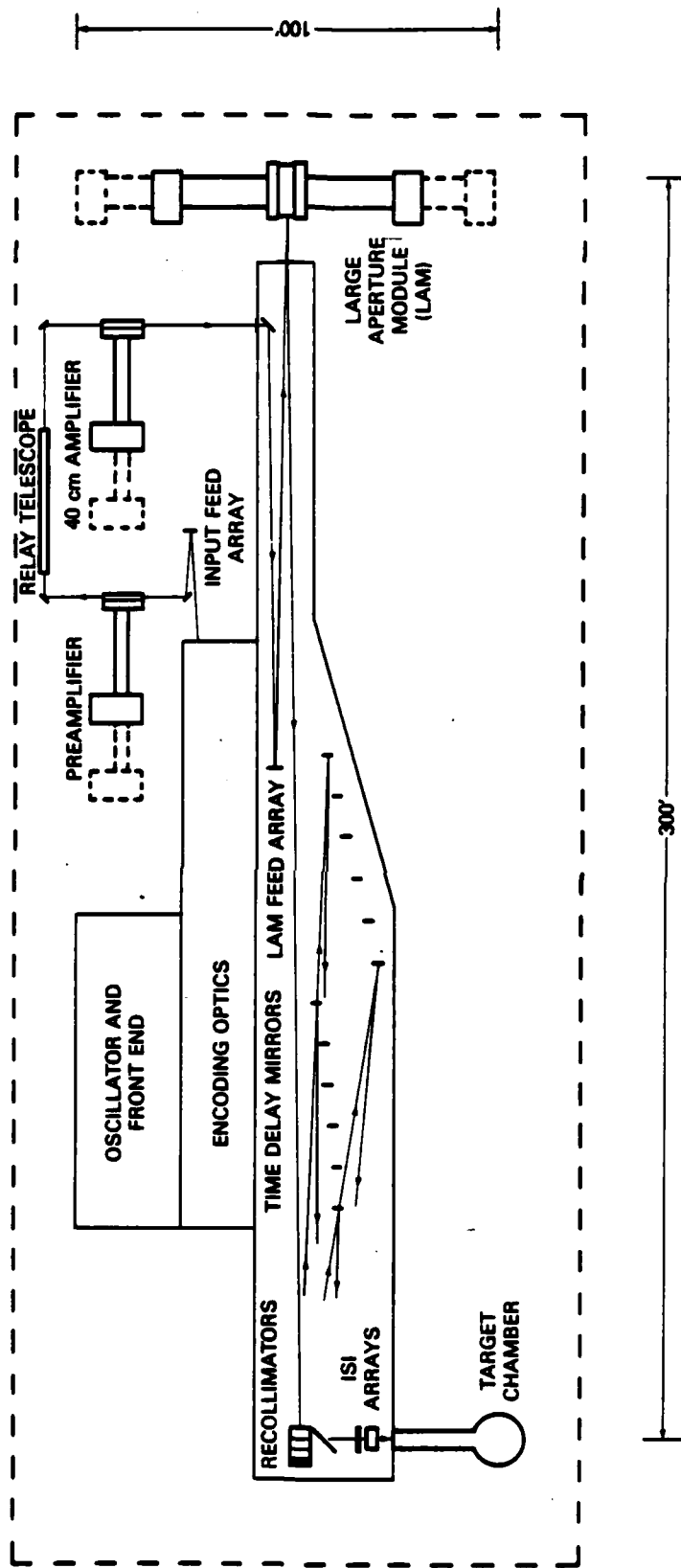
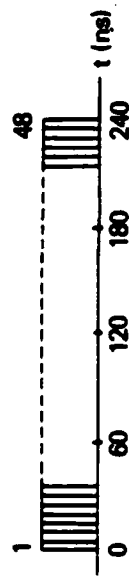
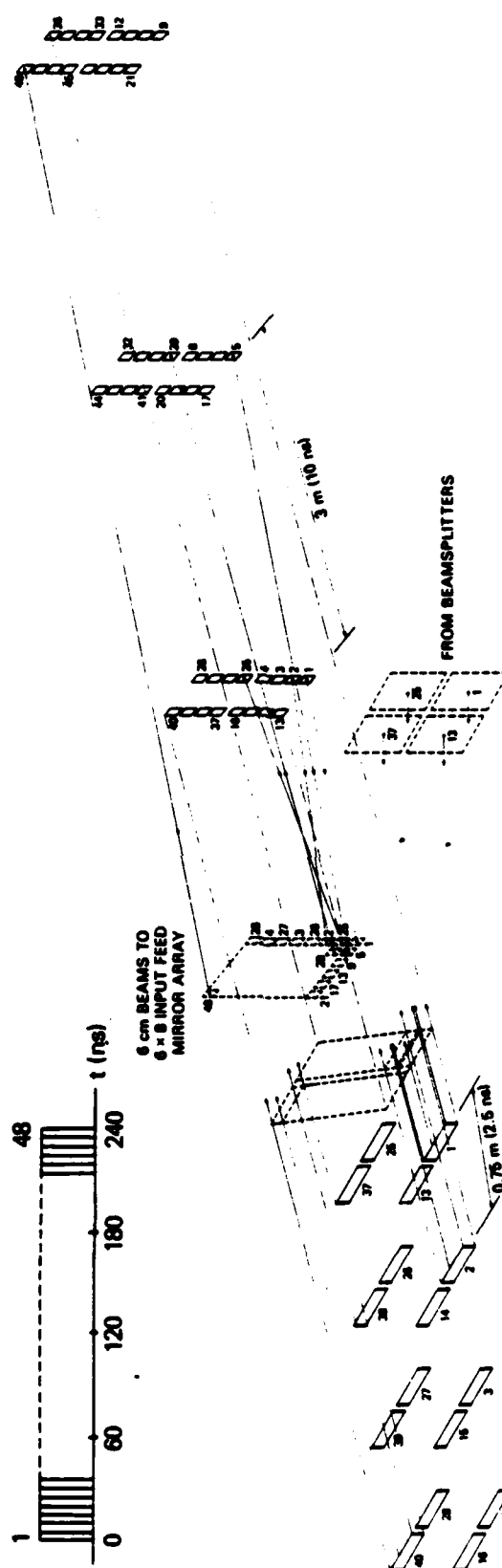


Fig. 6 — Floor plan for the proposed KrF laser

(b)

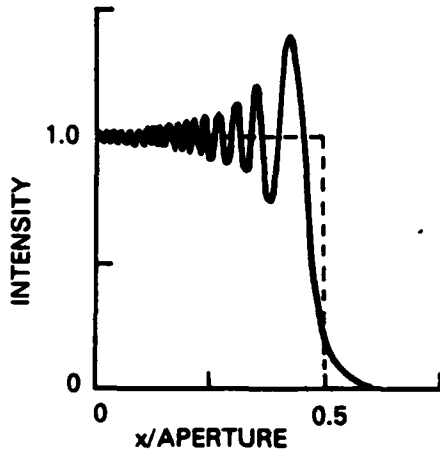


6 cm BEAMS TO
6 x 8 INPUT FEED
MIRROR ARRAY



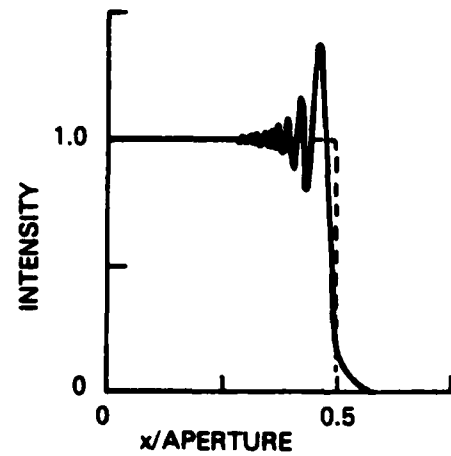
(a)

Fig. 8 — (a) Slicer arrays for producing a 6 x 8 matrix of sequential beams and (b) temporal sequence of the 48 5ns beams



USUAL CASE: SLICERS PLACED
BEFORE BEAMSPLITTERS
($z \approx 100\text{m}$, $N_F \approx 145$)

(a)



PROPOSED NRL SCHEME
($z \approx 30\text{ m}$, $N_F \approx 480$)

(b)

Fig. 9 — Fresnel diffraction patterns due to the hard aperture beam slicers. (a) Usual configuration, where the slicers would be placed before the beamsplitters ($N_F \approx 145$), (b) proposed NRL configuration shown in Figs. 8 and 9 ($N_F \approx 480$).

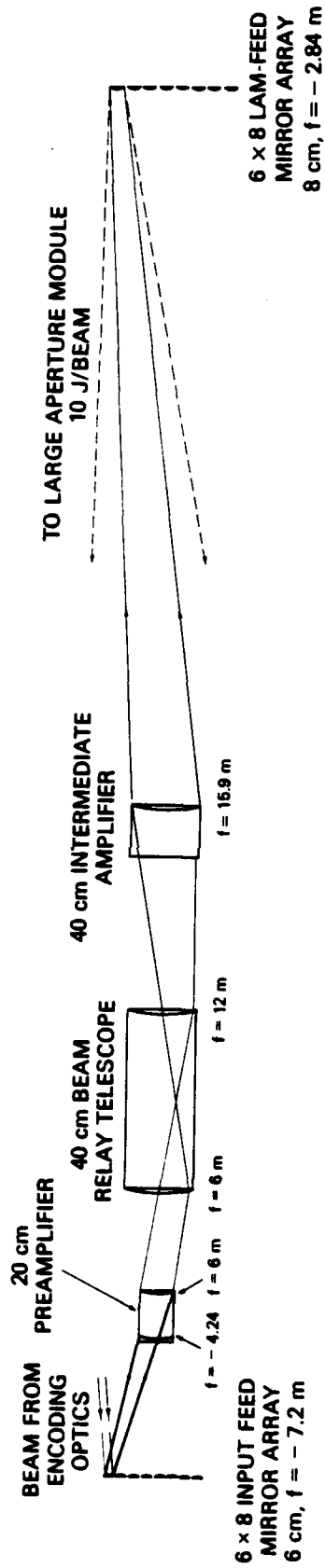
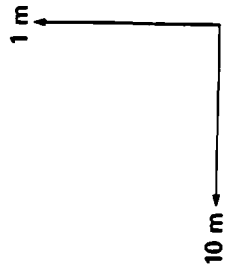


Fig. 10 — Schematic side view of the top row of beams propagating through the preamplifier and intermediate amplifier sections

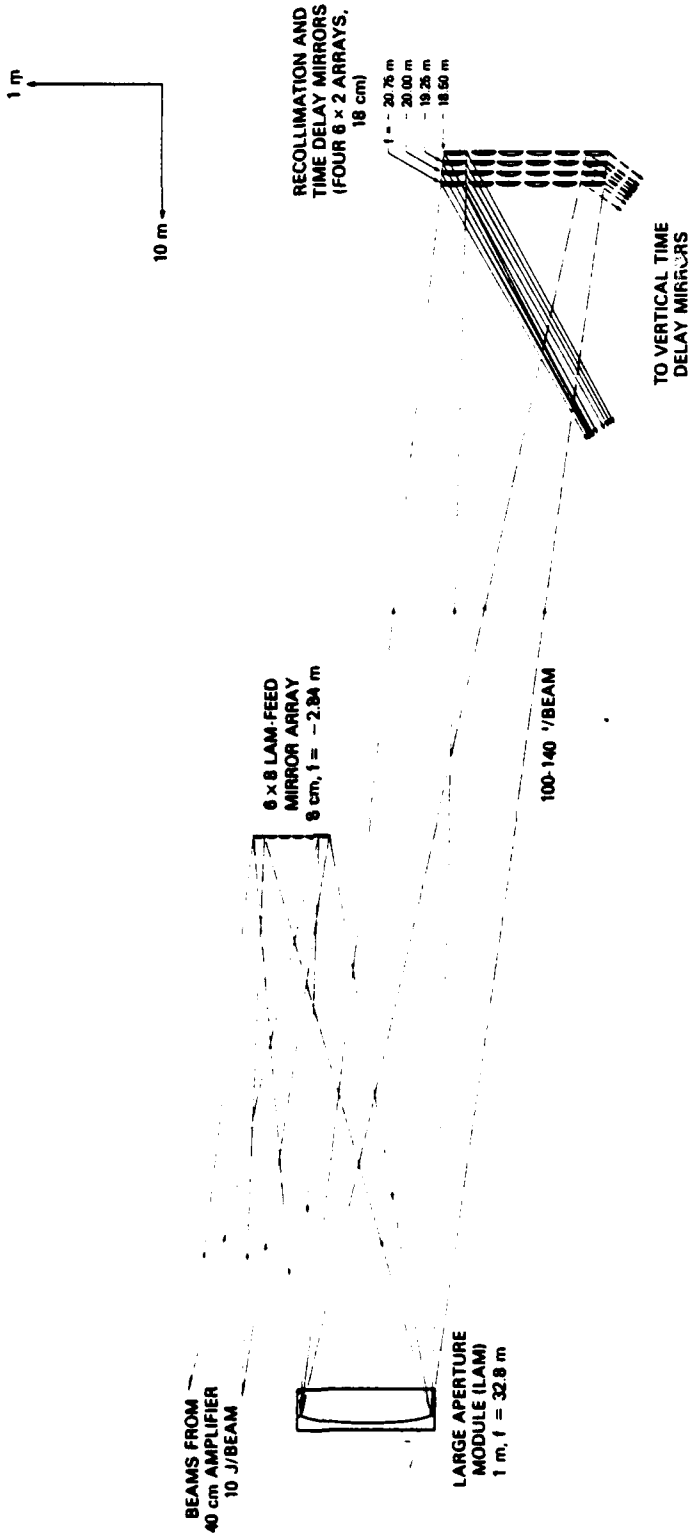
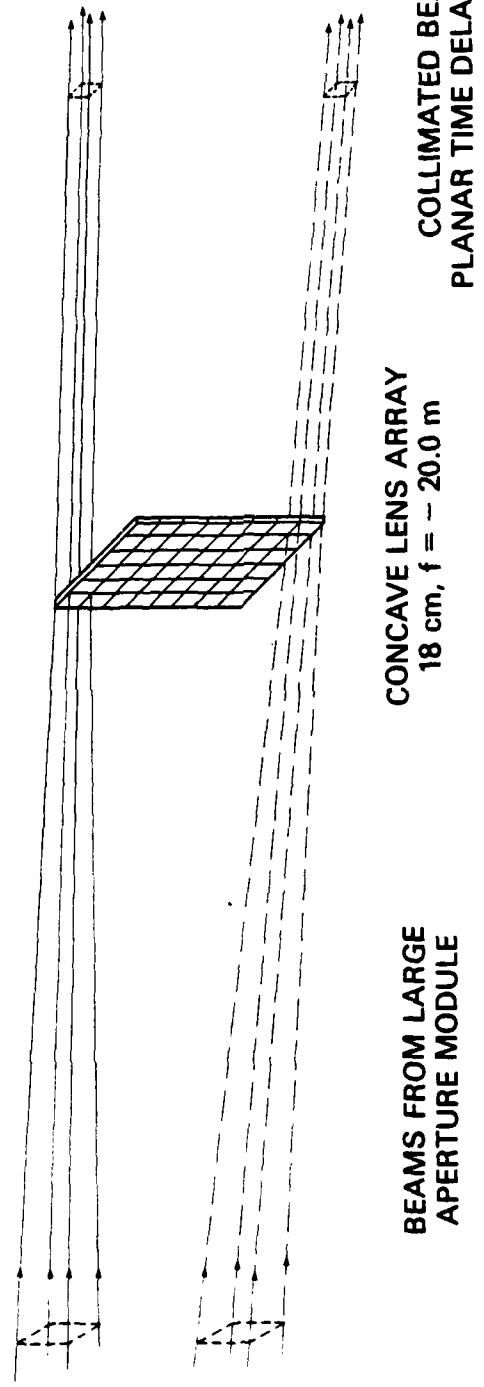


Fig. 11 — Schematic top view of the two outer columns of beams double-passing through the LAM to the recollimator mirrors



CONCAVE LENS ARRAY
 18 cm, $f = -20.0$ m

BEAMS FROM LARGE
 APERTURE MODULE

COLLIMATED BEAMS TO
 PLANAR TIME DELAY MIRRORS

Fig. 12 — Alternative recollimation scheme, using a concave lens array instead of the recollimator mirrors

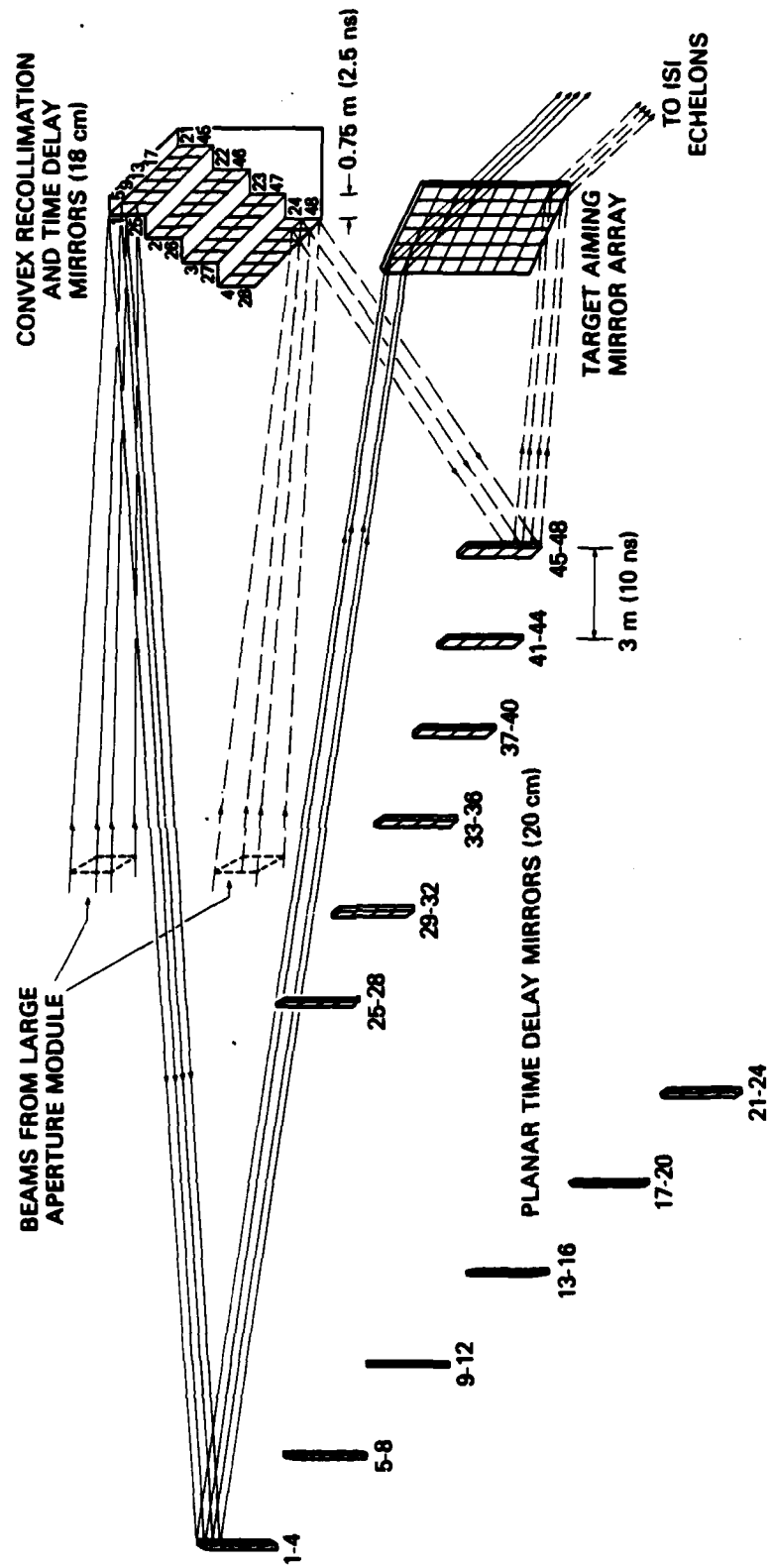


Fig. 13 — Decoding/recollimation optics

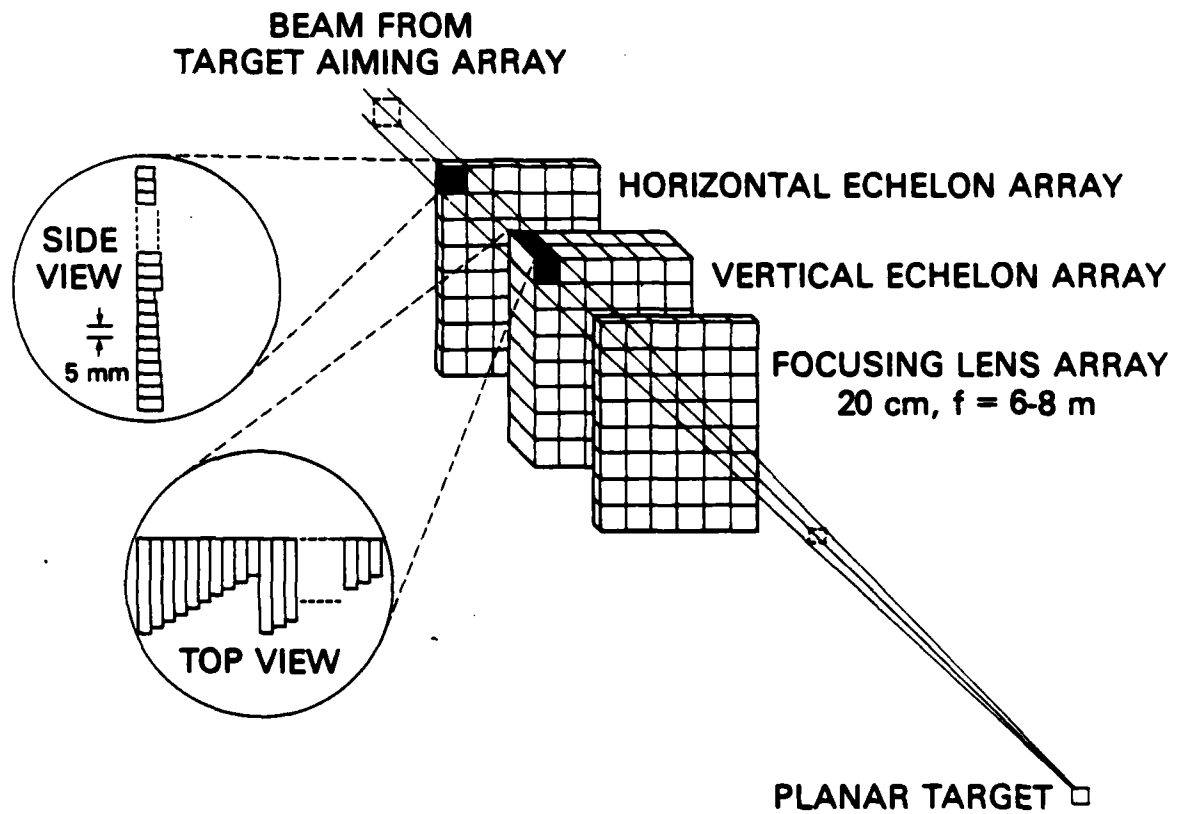
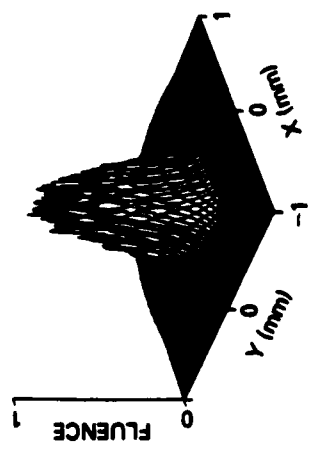
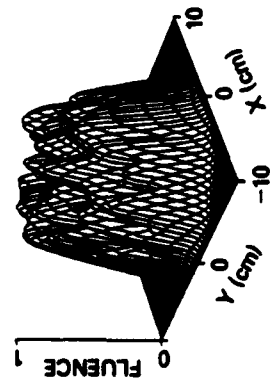
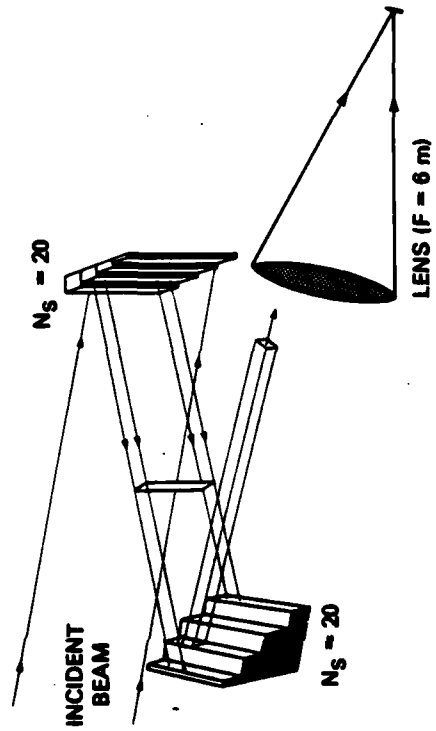
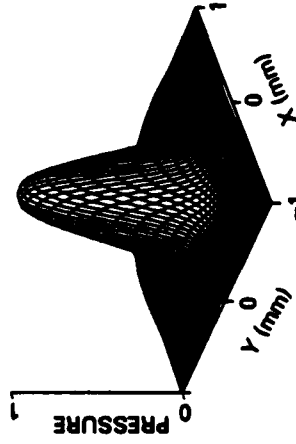


Fig. 14 — ISI and target focusing optics, showing detailed views of the horizontal and vertical echelons in each beam



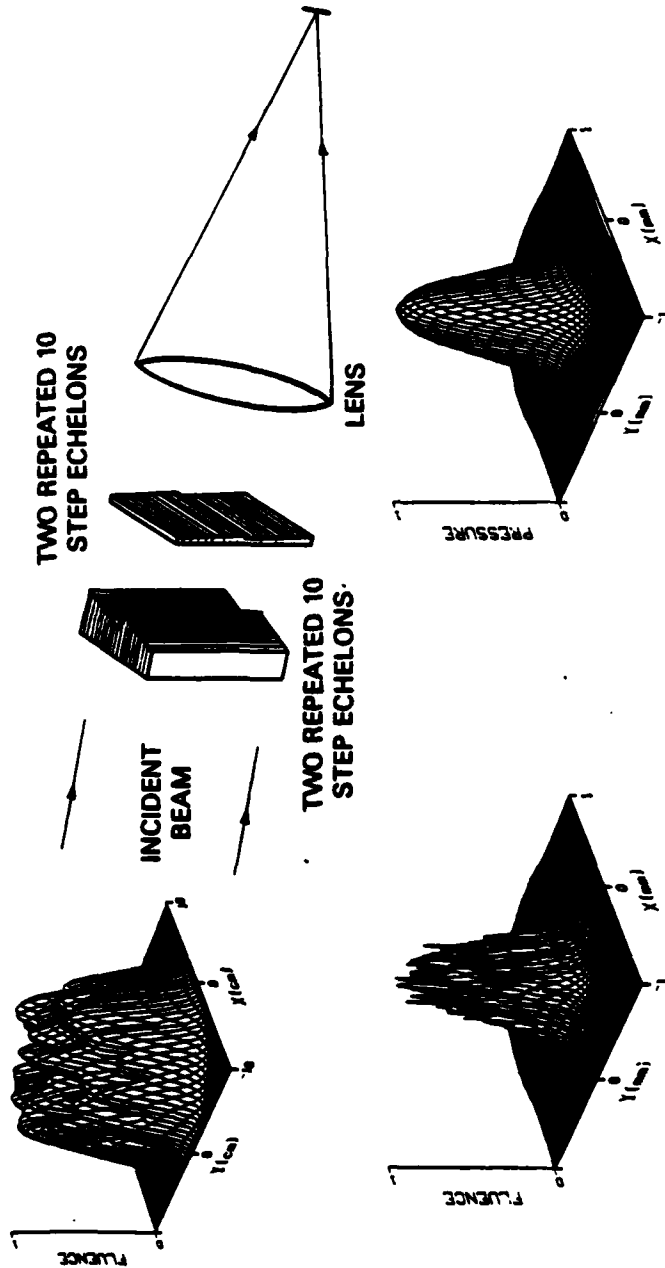
FOCAL POINT FLUENCE WITH THE ECHELONS IN PLACE, AND A BROADBAND LASER INTEGRATED OVER TIME INTERVAL $T = 100 t_c$.



ABLATION PRESSURE, ASSUMING THERMAL SMOOTHING WITH $\Delta R = 50 \mu\text{m}$. THE PEAK-TO-VALLEY DEVIATION FROM $\langle P \rangle$ IS 2.4%.

Fig. 15 - Numerical simulations of ISI with broadband $1/2 \mu\text{m}$ light: (a) incident laser beam, aberrated to $5 \times$ diffraction limit, (b) echelon/focusing configuration with 20 steps/echelon, (c) fluence at the focal plane (assumed to coincide with the plasma absorption region), integrated over 100 coherence times, and (d) ablation pressure, assuming thermal smoothing with a $50 \mu\text{m}$ absorption-ablation distance. The statistical deviation from ensemble-averaged pressure is 2.4% peak/valley.

PARTIAL ISI SCHEME USING REPEATED STEPS (RESULTS FOR ONE CHANNEL)



ABLATION PRESSURE, ASSUMING THERMAL SMOOTHING WITH $\Delta R = 50 \mu\text{m}$, THE PEAK-TO-VALLEY DEVIATION FROM $\langle P \rangle$ IS 3.9%.

FOCAL POINT FLUENCE WITH THE REPEATED ECHELONS AND A BROADBAND LASER INTEGRATED OVER TIME INTERVAL $T = 100 t_c$.

Fig. 16 - Numerical simulations of the partial ISI concept with broadband $1/2 \mu\text{m}$ light: (a) incident laser beam, aberrated to 5 \times diffraction limit, (b) echelon/focusing configuration with 20 steps/echelon in two 10 step segments, (c) fluence at the focal plane (plasma absorption region), integrated over 100 coherence times, and (d) ablation pressure, assuming thermal smoothing with a $50 \mu\text{m}$ absorption-ablation distance. The statistical deviation from ensemble-averaged pressure is 3.9%.

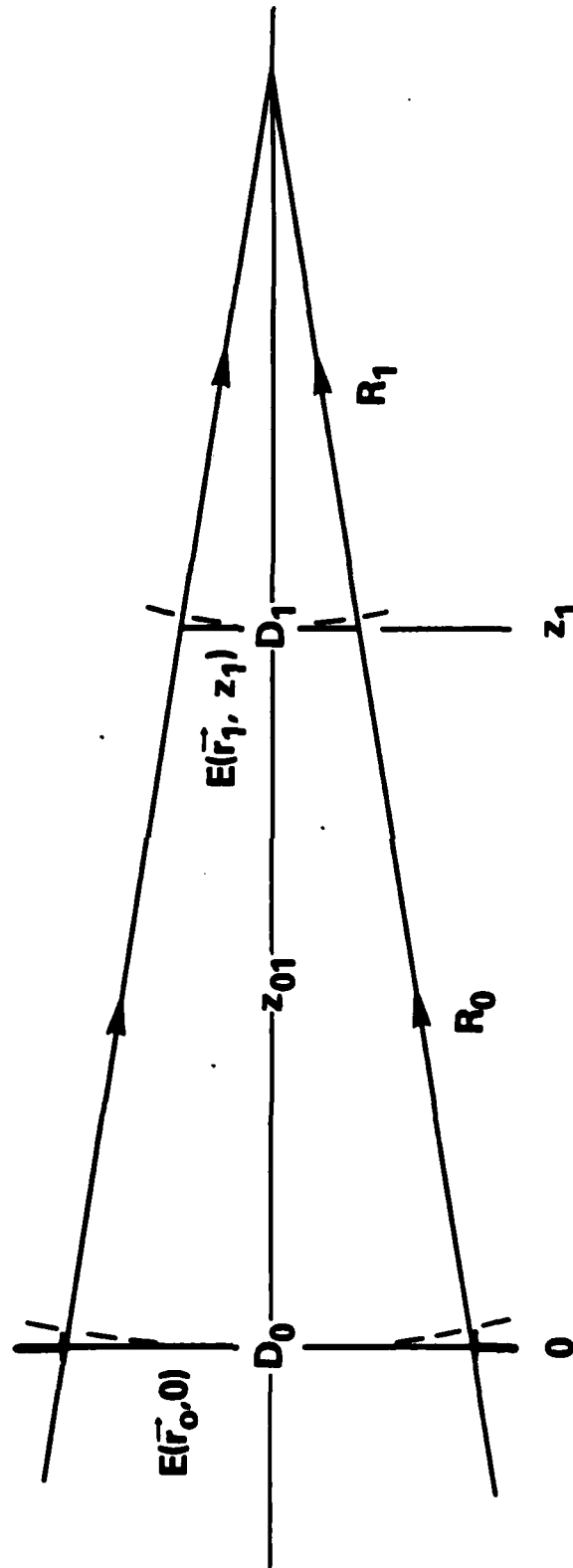


Fig. 17 — Ray diagram showing a converging optical field $E(\vec{r}_0, 0)$ traversing a square aperture at $z = 0$

END

FILMED

3

-86

DTIC